regimen for nonmalignant disorders. *Bone Marrow Transplant.* 2005;35(4):345-352.

9. Cooper N, Rao K, Gilmour K, et al. Stem cell transplantation with reduced-intensity conditioning for hemophagocytic lymphohistiocytosis. *Blood.* 2006;107(3):1233-1236.
10. Cooper N, Rao K, Goulden N, Webb D, Amrolia P, Veys P. The use of reduced-intensity stem cell transplantation in haemophagocytic lymphohistiocytosis and Langerhans cell histiocytosis. *Bone Marrow Transplant.* 2008;42(suppl 2):S47-50.
11. Marsh RA, Vaughn G, Kim MO, et al. Reduced-intensity conditioning significantly improves survival of patients with hemophagocytic lymphohistiocytosis undergoing allogeneic hematopoietic cell transplantation. *Blood.* 2010;116(26):5824-5831.
12. Lankester AC, Visser LF, Hartwig NG, et al. Allogeneic stem cell transplantation in X-linked lymphoproliferative disease: two cases in one family and review of the literature. *Bone Marrow Transplant.* 2005;36(2):99-105.
13. Booth C, Gilmour KC, Veys P, et al. X-linked lymphoproliferative disease due to SAP/SH2D1A deficiency: a multicenter study on the manifestations, management and outcome of the disease. *Blood.* 2011;117(1):53-62.
14. Kanegane H, Yang X, Zhao M, et al. Clinical features and outcome of X-linked lymphoproliferative syndrome type 1 (SAP deficiency) in Japan identified by the combination of flow cytometric assay and genetic analysis. *Pediatr Allergy Immunol.* 2012;23(5):488-493.
15. Rigaud S, Fondaneche MC, Lambert N, et al. XIAP deficiency in humans causes an X-linked lymphoproliferative syndrome. *Nature.* 2006; 444(7115):110-114.
16. Marsh RA, Madden L, Kitchen BJ, et al. XIAP deficiency: a unique primary immunodeficiency best classified as X-linked familial hemophagocytic lymphohistiocytosis and not as X-linked lymphoproliferative disease. *Blood.* 2010;116(7): 1079-1082.
17. Yang X, Kanegane H, Nishida N, et al. Clinical and genetic characteristics of XIAP deficiency in Japan. *J Clin Immunol.* 2012;32(3):411-420.
18. Worthey EA, Mayer AN, Syverson GD, et al. Making a definitive diagnosis: successful clinical application of whole exome sequencing in a child with intractable inflammatory bowel disease. *Genet Med.* 2011;13(3):255-262.
19. Duckett CS, Nava VE, Gedrich RW, et al. A conserved family of cellular genes related to the baculovirus iap gene and encoding apoptosis inhibitors. *EMBO J.* 1996;15(11):2685-2694.
20. Harlin H, Reffey SB, Duckett CS, Lindsten T, Thompson CB. Characterization of XIAP-deficient mice. *Mol Cell Biol.* 2001;21(10):3604-3608.
21. Jost PJ, Grabow S, Gray D, et al. XIAP discriminates between type I and type II FAS-induced apoptosis. *Nature.* 2009;460(7258):1035-1039.
22. Rumble JM, Oetjen KA, Stein PL, Schwartzberg PL, Moore BB, Duckett CS. Phenotypic differences between mice deficient in XIAP and SAP, two factors targeted in X-linked lymphoproliferative syndrome (XLP). *Cell Immunol.* 2009;259(1):82-89.
23. Fakler M, Loeder S, Vogler M, et al. Small molecule XIAP inhibitors cooperate with TRAIL to induce apoptosis in childhood acute leukemia cells and overcome Bcl-2-mediated resistance. *Blood.* 2009;113(8):1710-1722.
24. Schimmer AD, Estey EH, Borthakur G, et al. Phase I/II trial of AEG35156 X-linked inhibitor of apoptosis protein antisense oligonucleotide combined with idarubicin and cytarabine in patients with relapsed or primary refractory acute myeloid leukemia. *J Clin Oncol.* 2009;27(28):4741-4746.
25. Marsh RA, Villanueva J, Zhang K, et al. A rapid flow cytometric screening test for X-linked lymphoproliferative disease due to XIAP deficiency. *Cytometry B Clin Cytom.* 2009;76(5):334-344.
26. Bacigalupo A, Ballen K, Rizzo D, et al. Defining the intensity of conditioning regimens: working definitions. *Biol Blood Marrow Transplant.* 2009; 15(12):1628-1633.
27. Przepiorka D, Weisdorf D, Martin P, et al. 1994 Consensus Conference on Acute GVHD Grading. *Bone Marrow Transplant.* 1995;15(6):825-828.
28. Filipovich AH. Diagnosis and manifestations of chronic graft-versus-host disease. *Best Pract Res Clin Haematol.* 2008;21(2):251-257.
29. Shaw BE, Arguello R, Garcia-Sepulveda CA, Madrigal JA. The impact of HLA genotyping on survival following unrelated donor haematopoietic stem cell transplantation. *Br J Haematol.* 2010; 150(3):251-258.
30. Pachlopnik Schmid J, Canioni D, Moshous D, et al. Clinical similarities and differences of patients with X-linked lymphoproliferative syndrome type 1 (XLP-1/SAP deficiency) versus type 2 (XLP-2/XIAP deficiency). *Blood.* 2011;117(5): 1522-1529.

Journal of Receptors and Signal Transduction

http://informahealthcare.com/rst
ISSN: 1079-9893 (print), 1532-4281 (electronic)

J Recept Signal Transduct Res, 2013; 33(2): 124–128
 DOI: 10.3109/10799893.2013.779279

informa healthcare

RESEARCH ARTICLE

A novel *SOS1* mutation in Costello/CFC syndrome affects signaling in both RAS and PI3K pathways

Munkhtuya Tumurkhuu[1], Makiko Saitoh[1], Junko Takita[2,3], Yoko Mizuno[3], and Masashi Mizuguchi[1]

[1]*Department of Developmental Medical Sciences, Institute of International Health, Graduate School of Medicine,* [2]*Department of Cell Therapy and Transplantation Medicine, and* [3]*Department of Pediatrics, Faculty of Medicine, The University of Tokyo, Tokyo, Japan*

Abstract

Context: Pathological upregulation of the RAS/MAPK pathway causes Costello, Noonan and cardio–facio–cutaneous (CFC) syndrome; however, little is known about PI3K/AKT signal transduction in these syndromes. Previously, we found a novel mutation of the *SOS1* gene (T158A) in a patient with Costello/CFC overlapping phenotype. *Objective:* The aim of this study was to investigate how this mutation affects RAS/MAPK as well as PI3K/AKT pathway signal transduction.

Materials and methods: Wild-type and mutant (T158A) Son of Sevenless 1 (SOS1) were transfected into 293T cells. The levels of phospho- and total ERK1/2, AKT, p70S6K and pS6 were examined under epidermal growth factor (EGF) stimulation. *Results:* After EGF stimulation, the ratio of phospho-ERK1/2 to total ERK1/2 was highest at 5 min in mutant (T158A) SOS1 cells, and at 15 min in wild-type SOS1 cells. Phospho-AKT was less abundant at 60 min in mutant than in wild-type SOS1 cells. Phosphorylation at various sites in p70S6K differed between wild-type and mutant cells. Eighteen hours after activation by EGF, the ratio of phospho-ERK1/2 to total ERK1/2 remained significantly higher in mutant than in wild-type SOS1 cells, but that of phospho-AKT to total AKT was unchanged. *Discussion:* T158A is located in the histone-like domain, which may have a role in auto-inhibition of RAS exchanger activity of SOS1. T158A may disrupt auto-inhibition and enhance RAS signaling. T158A also affects PI3K/AKT signaling, probably via negative feedback via phospho-p70S6K. *Conclusion:* The *SOS1* T158A mutation altered the phosphorylation of gene products involved in both RAS/MAPK and PI3K/AKT pathways.

Keywords

Costello syndrome, noonan syndrome, PI3K/AKT pathway, RAS/MAPK pathway, *SOS1*

History

Received 21 January 2013
Revised 19 February 2013
Accepted 20 February 2013
Published online 26 March 2013

Introduction

Protein kinases and other messengers form highly interactive networks to achieve the integrated functions of cells. One of these critical signaling networks is a family known as rat sarcoma virus oncogene homologue (RAS)/mitogen-activated protein kinase (MAPK) cascade, which plays a major role in the regulation of embryogenesis, cell differentiation, proliferation and apoptosis (1,2).

Recently, germ-line mutations in RAS pathway genes have been recognized to cause Noonan, Costello and cardio–facio–cutaneous (CFC) syndromes (3–7). These syndromes share common clinical features, such as congenital heart defects, short stature, characteristic facial features and mental retardation. The activation of RAS is associated with its conversion from the GDP- to the GTP-bound form. Son of Sevenless 1 (SOS1) is a RAS-specific guanine nucleotide exchanger (8,9). Familial or *de novo* mutations in *SOS1* have been found in Noonan and CFC syndromes (5–7,10). Lepri et al. classified Noonan-associated *SOS1* mutations into three types: class 1 with predicted conformational rearrangements of domains, resulting in reduced enzyme auto-inhibition, class 2 with predicted enhancement of SOS1's catalytic function by membrane binding, and class 3 with mutations located in the catalytic domain (CDC25; Figure 1) (10). The mutations were inferred to disrupt auto-inhibition of RAS exchanger activity (class 1 and class 2), or to promote RAS binding to CDC25 (class 3), resulting in increased signal flow through RAS. The molecular pathogenesis of Noonan syndrome caused by a gain of function mutation in *SOS1* remains to be elucidated. A mouse carrying the *SOS1*E864K mutation shows many Noonan-like features (11). In the heart of these model mice, multiple signaling pathways are activated, including not only the RAS/MAPK pathway, but also Rac and Stat3. To better understand the pathogenesis of these syndromes, it is necessary to elucidate how various protein kinases are activated in a highly interactive network. To our knowledge, however, the activation status of the PI3K/AKT pathway in these syndromes has not been elucidated.

In a previous study, we found a novel *SOS1* mutation in a patient with Costello/CFC overlapping syndrome (12).

Address for correspondence: Makiko Saitoh, Department of Developmental Medical Sciences, Institute of International Health, Graduate School of Medicine, The University of Tokyo, Bunkyo-ku, 7-3-1, 113-0033 Tokyo, Japan. Tel: +81-3-5841-3615. Fax: +81-3-5841-3628. E-mail: makisaito-tky@umin.ac.jp

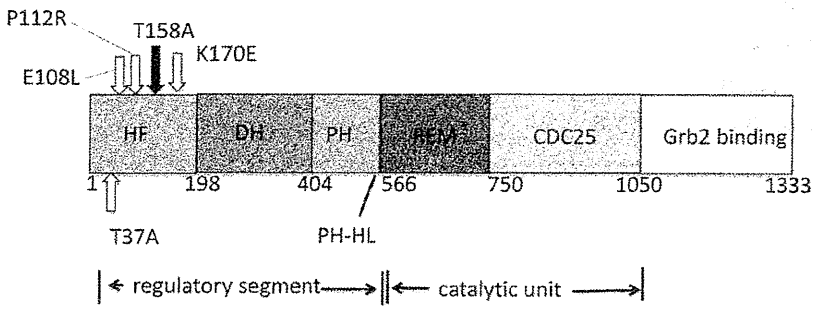

Figure 1. SOS1 domain structure and location of identified amino acid substitutions in HF domain of SOS1. The functional domains of SOS1 are as follows: DH, DBL homology; PH, pleckstrin homology; HL, helical linker; REM, RAS exchange motif; CDC25, RAS guanine nucleotide exchange factor and Grb2 binding. HF, DH, PH and HL constitute a regulatory segment, whereas REM and CDC25 form a catalytic unit. Previously reported variants in HF domain (white arrows) are K170E (class 1), E108L (class 2) and P112R (class 2). Effect of T37A on SOS1 function is unknown. T158A (black arrow) is a novel mutation found by our previous study.

This mutation caused substitution from threonine to alanine at position 158 located in the histone-like fold (HF) domain (Figure 1). This mutation is located close to a previously reported mutation K170E, which is predicted to cause conformational rearrangement of domains, resulting in reduced enzyme auto-inhibition (10). In this study, we investigated whether the *SOS1* T158A mutation can activate the RAS/MAPK pathway to cause Costello/CFC syndrome. Human embryonic kidney 293T cells were transfected with wild-type human SOS1 and mutant (T158A) isoform SOS1. Using these cells, we studied the phosphorylation of ERK1/2 and AKT under stimulation by epidermal growth factor (EGF).

Materials and methods

We expressed wild-type SOS1 and mutant T158A SOS1 in human embryonic kidney 293T cells and measured the phosphorylation level of downstream effectors of the RAS/MAPK pathway, such as extracellular signal-regulated kinase1/2 (ERK1/2), and ribosomal protein S6 (pS6), as well as that of v-Akt murine thymoma viral oncogene homolog (AKT), the main regulator of the PI3K/AKT pathway, and ribosomal protein S6 kinase, 70KDa (p70S6K). Human embryonic kidney 293T cells were maintained in Dulbecco's modified Eagle's medium (DMEM) plus 10% fetal bovine serum (FBS) and antibiotics. Human *SOS1* containing plasmid was purchased from NITE Biological Resource Center (Osaka, Japan). The primers were designed to amplify target mutation (forward: SOS1Mut1F: ATATACG GCATTATGAAATTGCAAAACAAGATAT and reverse: SOS1Mut1R: AATTTCATAATGCCGTATATTTCTTACAT AAT). We generated Costello/CFC syndrome-associated *SOS1* mutant T158A using the Gene Tailor site-directed mutagenesis system (Invitrogen, Carlsbad, CA) according to the manufacturer's protocol. Wild-type and T158A mutant plasmids were transfected into DH5αTM-T1R *Escherichia coli*. By sequencing the picked-up colonies, we confirmed the T158A mutation. Wild-type or mutant T158A *SOS1* expression constructs were transfected into 293T cells using MultiFectam reagent (Promega, Madison, WI). One day prior to transfection, the cells were plated in six-well plates at a density of 1×10^5 cells per well and were grown to 85% confluence. Plasmid DNA (2.5 μg) containing either wild-type or mutant *SOS1* was suspended with 125 μl of 20 mM Tris-HCl buffer (pH 7.4). Then, 62.5 μl MultiFectam reagent was added to the plasmid solution and was incubated for 30 min at room temperature, followed by the addition of 62.5 μl serum-free DMEM medium. For transfection, 293 T cells were incubated in this mixture for 4 h and then in complete DMEM medium with 10% FBS for 24 h. Next, for EGF stimulation, cells were cultured in DMEM without serum for 18 h. EGF (100 ng/ml medium) was then added and incubated for 5, 15 and 30 min. We determined the level of phospho-ERK1/2, phospho-pS6, phospho-AKT and phospho-p70S6K at 5, 15 and 60 min after the onset of stimulation by EGF. All the cells were scraped, collected and washed twice with phosphate-buffered saline, pH 7.4, and suspended in TS buffer (0.5 ml of 1 M Tris HCl, pH 7.7, 1.5 ml of 1 M NaCl, 1 ml of 500 mM EDTA, 7 ml distilled water containing 100 μl protease inhibitor mixture (GE Healthcare, Little Chalfont, Buckinghamshire, UK) and sonicated on ice for 15 s. The lysates were centrifuged at 12 000 g for 30 min at 4 °C, and the protein concentration of their supernatant was determined by the Bradford assay. We also examined the effect of mutant SOS1 transfection on the phosphorylation of ERK1/2 with a longer interval after EGF stimulation. The 293T cells were first stimulated by EGF in DMEM plus 10% FBS for 20 min and then cultured in serum-free DMEM for 18 h. To verify the overexpression of transfected SOS1 in 293T cells, an antibody against SOS1 (Santa Cruz Biotechnology Inc., Santa Cruz, CA) was used. ERK1/2, AKT and pS6 activations were detected by immunoblotting with antibodies against phosphorylated ERK (phospho-ERK) (Thr202/Tyr204), phosphorylated AKT (phospho-AKT) (Ser473), phosphorylated-p70S6K (phospho-p70S6K) (Thr389), phospho-p70S6K (Thr421/Ser424) and phosphorylated pS6 (phospho-pS6) (Ser235/236) purchased from Cell Signaling Technology (Beverly, MA). Band intensities were quantified using Image J software (version 1.44, NIH). For statistical analysis, data were collected from at least three independent experiments and compared using Student's *t* test. Statistical significance was determined as $p < 0.05$.

This study was approved by the Ethics Committee of the University of Tokyo.

Results

On Western blots, the 150 kDa band corresponded to the full-length SOS1. The amount of SOS1 was at least three times as high in cells transfected with mutant (T158A) SOS1 as in non-transfected cell lines (Figure 2, upper left panel). The weak SOS1 immunoreactivity of non-transfected cells

J Recept Signal Transduct Res, 2013; 33(2): 124–128

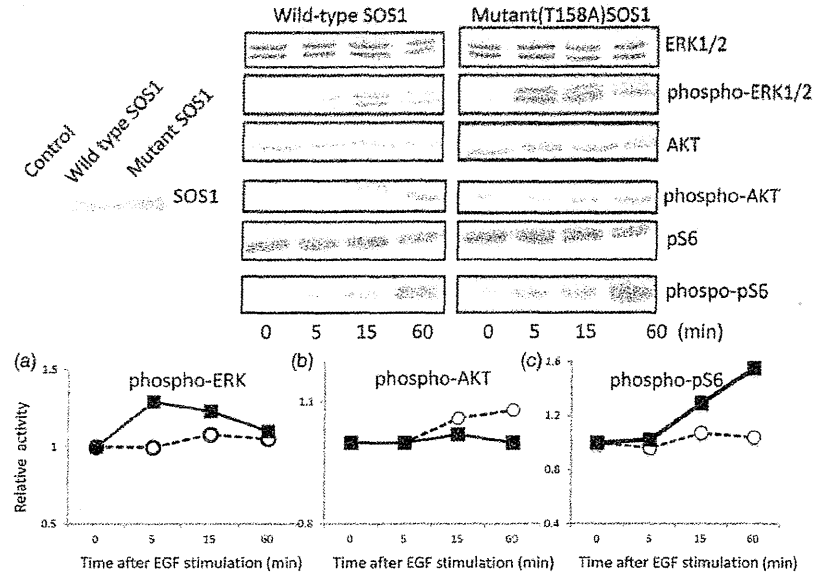

Figure 2. SOS1 T158A mutation alters early response of ERK/AKT/pS6 to EGF. The amount of the SOS1 protein was larger in cell lines overexpressing wild-type and mutant (T158A) SOS1 than in non-transfected, control cell lines (upper left panel). Upper right panels show ERK1/2, AKT and pS6 activation in cells expressing wild-type and mutant SOS1 that were starved and stimulated with EGF for 0–30 min. Lower panels show relative activity of ERK1/2, AKT and pS6 corrected by the ratio of phospho-protein to total protein at basal stage (0 min). (a) The peak of ERK1/2 phosphorylation was higher in mutant (closed square) than in wild-type SOS1 cells (open circle). (b) At 60 min, phosphorylation of AKT at was elevated in wild-type SOS1 cells, but remained unchanged in mutant cells. (c) Phosphorylation of pS6 was higher in mutant SOS1 cells than in wild-type SOS1 cells.

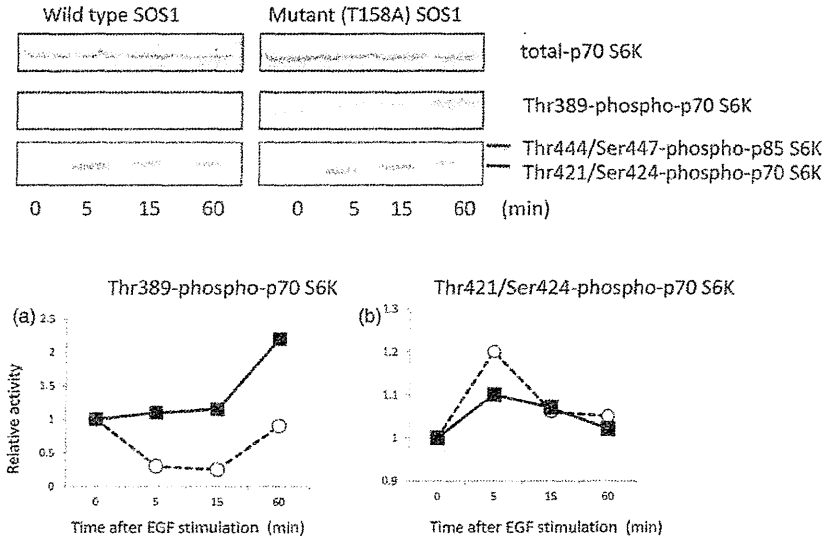

Figure 3. SOS1 T158A mutant alters the late response of p70S6K to EGF. Phosphorylation of p70S6K at various phosphorylation sites is shown in upper panel. (a) Sixty minutes after stimulation of EGF, phosphorylation of p70S6K at Thr 389 is elevated in mutant SOS1 cells. (b) Five minutes after EGF stimulation, phosphorylation of p70S6K at Thr421/Ser424 was higher in wild-type (open circle) than in mutant SOS1 cells (closed square). Phosphorylation of p85S6K at Thr444/Ser447 was detectable in mutant but not in wild-type SOS1 cells.

was considered to have resulted from endogenous expression of SOS1 protein. There was no difference between cells transfected with wild and mutated SOS1 protein.

Changes of total and phospho-ERK1/2, AKT and pS6 in 293T cells after EGF stimulation were studied by Western blotting (Figure 2, upper right panels). Western blotting of total and phospho-ERK1/2 detected 42 and 44 kDa bands, respectively. Although the basal level of phospho-ERK1/2 was low, it increased rapidly after EGF treatment (Figure 2a). The ratio of phospho-ERK1/2 to total ERK1/2 was highest 5 min after EGF stimulation in mutant SOS1 cells, while it was highest at 15 min in wild-type SOS1 cells. Phospho-AKT was barely detectable in wild-type SOS1 cells under basal conditions as well as 5 and 15 min after stimulation. Sixty minutes after stimulation, it became clearly detectable and was less abundant in mutant SOS1 cells than in wild-type SOS1 cells (Figure 2b). The increase of phospho-pS6 was more prominent and earlier in mutant SOS1 cells than in wild-type SOS1 cells (Figure 2c).

Next, to explore the reason for the effects of this mutation on AKT, we investigated the phosphorylation of p70S6K. As shown in Figure 3 (upper panel and (a)), the level of phosphorylation at Thr389 was higher in mutant SOS1 cells, but low in wild-type SOS1 cells. The phosphorylation level of Thr444/Ser447-p85S6K, an isoform of p70S6K was detectable in mutant, but not in wild-type SOS1 cells. The ratio of Thr421/Ser424-phospho-p70S6K to total-p70S6K 5 min after EGF stimulation was higher in wild-type than in mutant SOS1 cells (Figure 3b).

When the cells were starved for 18 h after stimulation by 100 ng/ml EGF, the level of phospho-ERK1/2 was significantly higher in mutant than in wild-type SOS1 cells (Figure 4, left panel), suggesting that mutant SOS1 remained active continuously, leading to higher RAS activity in

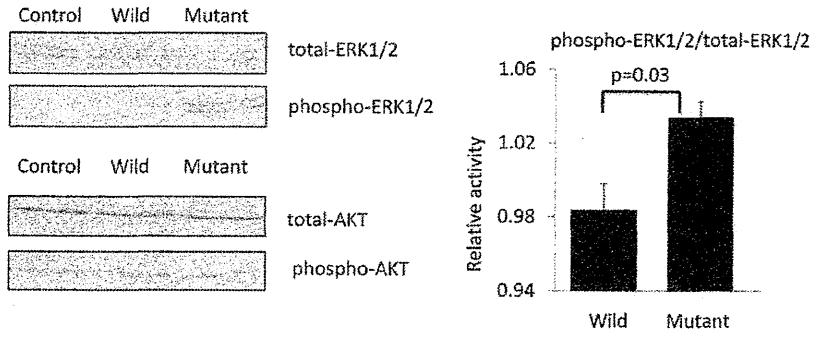

Figure 4. SOS1 T158A mutation causes prolonged activation of ERK1/2. After stimulation by EGF for 18 h, the level of phospho-ERK1/2 in the mutant SOS1 transfected cells were significantly higher than in the wild type SOS1 transfected cells, whereas that of phospho-AKT was comparable between them. The quantitative analysis (right) was based on the results of five independent experiments.

response to growth factor stimuli. The ratio of phospho- to total ERK1/2 was significantly higher in mutant than in wild-type SOS1 cells (Figure 4, right panel) ($p = 0.03$). There was no difference in the expression level of phospho-AKT 18 h after stimulation with EGF.

Discussion

In this study, we showed that *SOS1* T158A mutation causes hyper-activation of ERK1/2 in the RAS/MAPK pathway. T158A is located in the HF domain, the N-terminal segment of SOS1 that shows clear sequence similarity to histone (Figure 1). Functional analysis of mutated SOS1 with amino acid substitution in the HF domain has been reported previously (13,14). Induced mutations in the HF domain (Asp-140 and Asp-169) *in vitro* completely abolish the interaction between the isolated HF domain and other domains (14). Since the T158A mutation located in HF domain is a novel mutation that has never been reported in Costello, Noonan and CFC syndromes, we carried out a functional study to assess whether this mutation indeed alters the activation status of the RAS/MAPK pathway, as well as that of the PI3K/AKT pathway.

When we over-expressed SOS1 in 293T cells, the increase of ERK activation after EGF stimulation was faster and stronger with mutant T158A than with wild-type SOS1-transfected cells. Expression of T158A also resulted in constitutive RAS activation 18 h after EGF stimulation. Induction by EGF elicited a stronger response, both in magnitude and duration, indicating the functional consequence of the SOS1 mutation in 293T cells. These results confirmed our prediction that T158A mutation will abrogate auto-inhibition of SOS1 protein, thereby resulting in increased downstream signaling of the RAS/MAPK pathway.

The present study showed that, in the early response to EGF, phosphorylation of both ERK1/2 and p70S6K, the effectors of the RAS/MAPK pathway, was higher in mutant than in wild-type SOS1 cells. Although PI3K/AKT signaling was activated by EGF both in mutant and wild-type SOS1 cells, AKT activation was lower in mutant SOS1 cells. This finding is explained on the basis of a feedback mechanism in which activated p70S6K phosphorylates insulin receptor substrate-1 (IRS-1) to inhibit PI3K and AKT activation (15,16). The activity of p70S6K is controlled by multiple phosphorylation events located within the catalytic, linker and auto-inhibitory domains (17). Phosphorylation at Thr389 in the linker domain and at Thr421/Ser424 in the auto-inhibitory domain by mitogen-stimulated kinase in the RAS pathway precedes the activation of catalytic domain of p70S6K (17,18). In the late response to EGF, AKT activation was absent in both wild-type and mutant SOS1 cells.

The present study shows that *SOS1* T158A mutation affects both the RAS/MAPK and PI3K/AKT pathway by altering ERK and AKT phosphorylation. Activation of the RAS, PI3K, Src, PLCγ and other signaling pathways may alter cell fate after growth factor stimuli (19). To monitor their external and internal situations, cells use multiple pathways that are integrated at specific signaling steps (20,21). In PC12 cells, NGF induces combined phospho-ERK and phospho-AKT signal variation that enables a decision on differentiation and/or proliferation (22). Therefore, dysregulation in RAS/MAPK as well as PI3K/AKT signal transduction, caused by T158A SOS1 mutation, may affect the balance between cellular differentiation and proliferation and produce the clinical phenotypes of Costello/CFC syndrome.

Conclusion

The *SOS1* mutation T158A causes excessive activation of the RAS/MAPK pathway, as well as attenuated activation of AKT, in response to EGF stimulation. Altered signal transduction in the RAS/MAPK as well as PI3K/AKT pathway may account for the variable clinical expression of overlapping syndromes of the RAS/MAPK pathway.

Declaration of interest

The authors report no conflicts of interest.

Supported in part by Grants-in-Aid for Scientific Research from the Japan Society for the Promotion of Science (Nos. 20390293 and 22659190), and by a Grant-in-Aid for research (H23-Nanji-Ippan-31) from the Ministry of Health, Labour and Welfare, Japan.

References

1. Barbacid M. RAS genes. Annu Rev Biochem 1987;56:779–82.
2. Downward J. Targeting RAS signalling pathways in cancer therapy. Nat Rev Cancer 2003;3:11–22.
3. Aoki Y, Niihori T, Kawame H, et al. Germline mutations in HRAS proto-oncogene cause Costello syndrome. Nat Gene 2005;37:1038–40.
4. Zenker M, Lehmann K, Schulz AL, et al. Expansion of the genotypic and phenotypic spectrum in patients with KRAS germline mutations. J Med Genet 2006;44:131–5.
5. Roberts AE, Araki T, Swanson KD, et al. Germline gain-of-function mutations in SOS1 cause Noonan syndrome. Nat Genet 2007;39:70–4.

6. Tartaglia M, Pennacchio LA, Zhao CY, Gain-of-function SOS1 mutations cause a distinctive form of Noonan syndrome. Nat Genet 2007;39:75–9.
7. Narumi Y, Aoki Y, Niihori T, et al. Clinical manifestations in patients with SOS1 mutations range from Noonan syndrome to CFC syndrome. J Hum Genet 2008;53:834–41.
8. Boriack-Sjodin PA, Margarit SM, Bar-Sagi D, Kuriyan J. The structural basis of the activation of Ras by Sos. Nature 1998;394: 337–43.
9. Schlessinger J. Cell signaling by receptor tyrosine kinases. Cell 2000;103:211–25.
10. Lepri F, De Luca A, Stella L, et al. SOS1 mutations in Noonan syndrome: molecular spectrum, structural insights on pathogenic effects, and genotype-phenotype correlations. Hum Mut 2011;32: 760–72.
11. Chen PC, Wakimoto H, Conner D, et al. Activation of multiple signaling pathways causes developmental defects in mice with a Noonan syndrome-associated Sos1 mutation. J Clin Invest 2010; 120:4353–65.
12. Tumurkhuu M, Saitoh M, Sato A, et al. A comprehensive genetic analysis of overlapping syndromes of RAS/RAF/MEK/ERK pathway. Pediatr Int 2010;52:557–62.
13. Sondermann H, Soisson SM, Bar-Sagi D, Kuriyan J. Tandem histone folds in the structure of the N-terminal segment of the RAS activator Son of Sevenless. Structure 2003;11: 1583–93.
14. Sondermann H, Soisson SM, Boykevicsh M, et al. Structural analysis of autoinhibition in the RAS activator Son of Sevenless. Cell 2004;119:393–405.
15. Bilanges B, Vanhaesebroeck B. A new tool to dissect the function of p70 S6 kinase. Biochem J 2011;431:e1–3.
16. Harrington LS, Findlay GM, Gray A, et al. The TSC1-2 tumor suppressor controls insulin–PI3K signaling via regulation of IRS proteins. J Cell Biol 2004;166:213–23.
17. Pullen N, Dennis PB, Andjelkovic M, et al. Phosphorylation and activation of $p70^{s6k}$ by PDK1. Science 1998;279:707–10.
18. Dennis PB, Pullen N, Pearson RB, et al. Phosphorylation sites in the autoinhibitory domain participate in p70S6K activation loop phosphorylation. J Biol Chem 1998;273:14845–52.
19. Lemmon MA, Schlessinger J. Cell signaling by receptor tyrosine kinases. Cell 2010;141:1117–34.
20. Albert R. Scale-free networks in cell biology. J Cell Sci 2005;118: 4947–57.
21. Barabasi AL, Oltvai ZN. Network biology: understanding the cell's functional organization. Nat Rev Genet 2004;5:101–13.
22. Chen JY, Lin JR, Cimprich KA, Meyer T. A two-dimensional ERK-AKT signaling code for an NGF-triggered cell-fate decision. Mol Cell 2012;45:196–209.
23. Ko JM, Kim JM, Kim GH, Yoo HW. PTPN11, SOS1, KRAS, and RAF1 gene analysis, and genotype-phenotype correlation in Korean patients with Noonan syndrome. J Hum Genet 2008;53: 999–1006.

Aggressive Transformation of Juvenile Myelomonocytic Leukemia Associated with Duplication of Oncogenic *KRAS* due to Acquired Uniparental Disomy

Motohiro Kato, MD, PhD[1,*], Naoko Yasui, MD[1,*], Masafumi Seki, MD[2,*], Hiroshi Kishimoto, MD[3], Aiko Sato-Otsubo, MS[4], Daisuke Hasegawa, MD, PhD[5], Nobutaka Kiyokawa, MD, PhD[6], Ryoji Hanada, MD[1], Seishi Ogawa, MD, PhD[4], Atsushi Manabe, MD, PhD[5], Junko Takita, MD, PhD[2,7], and Katsuyoshi Koh, MD[1]

A small fraction of cases of juvenile myelomonocytic leukemia (JMML) develop massive disease activation. Through genomic analysis of JMML, which developed in an individual with mosaicism for oncogenic *KRAS* mutation with rapid progression, we identified acquired uniparental disomy at 12p. We demonstrated that duplication of oncogenic *KRAS* is associated with rapid JMML progression. *(J Pediatr 2013;* ■*:* ■*-* ■*).*

Juvenile myelomonocytic leukemia (JMML) is a rare pediatric myeloproliferative disorder, characterized by malignant transformation in the stem cell compartment with clonal proliferation of progeny that variably retain the capacity to differentiate. The clinical course of JMML is heterogeneous. Some patients require prompt allogeneic hematopoietic stem cell transplantation, whereas some demonstrate a milder clinical course, and some of them eventually exhibit spontaneous improvement.[1] Recent investigations into the molecular pathogenesis of JMML revealed that approximately 80% of patients harbored mutually exclusive mutations in genes regulating the Ras-mitogen-activated protein kinase (MAPK) pathway, including *RAS*, *PTPN11*, *NF1*, and *CBL*, leading to aberrant activation of the Ras-MAPK pathway.[1,2] The spectrum of mutations described thus far in JMML provides potential new opportunities for both diagnosis and therapy.

Previous studies reported that a small fraction of patients with JMML develop rapid and massive disease activation after an indolent clinical course. A report showed the incidence of progression to blastic phase to be 13%.[3] The etiology of the aggressive transformation remains unelucidated, however. We present a patient with JMML with a *KRAS* mutation who developed aggressive transformation and died. We performed genomic analysis to investigate the molecular pathology of this rapid and fatal progression.

Methods

A 1-year-old boy presented with leukocytosis (white blood cell count 46 800/mm^3, 20% monocytes, no blast cells) and hepatosplenomegaly. Bone marrow aspiration revealed hypercellular marrow, with 0.5% blast cells. Karyotyping was normal, and reverse-transcription polymerase chain reaction detected no *BCR-ABL* fusion. Fetal hemoglobin concentration was elevated (22%). Spontaneous growth of colony-forming unit granulocyte macrophages and hypersensitivity to granulocyte macrophage colony-stimulating factor were demonstrated, and mutation analysis revealed a heterozygous *KRAS* mutation (G12D: GGT>GAT) in peripheral blood mononuclear cells (PBMCs), all of which were consistent with JMML.[4] By 2 months after diagnosis, leukocytosis and hepatosplenomegaly had progressed. Oral 6-mercaptopurine (6-MP) therapy was started, and the patient remained stable for the next 10 months.

At 1 year after diagnosis, the patient suddenly developed tachypnea, impaired consciousness, and massive hepatosplenomegaly. Laboratory data revealed a white blood cell count of 124 400/mm^3 (38% monocytes, 5% blast cells; Figure 1, A). The patient's condition deteriorated rapidly, and he died from respiratory dysfunction. Autopsy revealed dysplastic cells infiltrating the bone marrow, lymph nodes, central nervous system, lungs, liver, spleen, pancreas, and kidneys (Figures 1, B and 2; Figure 2 available at www.jpeds.com).

Our genomic analysis was approved by the Ethics Board of the University of Tokyo, and informed consent was obtained from the child's guardian. Direct sequencing of the *KRAS* gene was performed for his normal muscle, heart, and lung (obtained at autopsy) and for PBMCs at diagnosis and at progression. Genome-wide analysis for genetic lesions was performed by single nucleotide polymorphism (SNP) array analysis. DNA

6-MP	6-mercaptopurine
JMML	Juvenile myelomonocytic leukemia
MAPK	Mitogen-activated protein kinase
PBMC	Peripheral blood mononuclear cell
SNP	Single nucleotide polymorphism
UPD	Uniparental disomy

From the [1]Department of Hematology/Oncology, Saitama Children's Medical Center, Saitama, Japan; [2]Department of Pediatrics, Graduate School of Medicine, University of Tokyo, Tokyo, Japan; [3]Department of Pathology, Saitama Children's Medical Center, Saitama, Japan; [4]Cancer Genomics Project, Graduate School of Medicine, University of Tokyo, Tokyo, Japan; [5]Department of Pediatrics, St Luke's International Hospital, Tokyo, Japan; [6]Department of Pediatric Hematology and Oncology Research, National Research Institute for Child Health and Development, Tokyo, Japan; and [7]Department of Cell Therapy and Transplantation Medicine, Graduate School of Medicine, University of Tokyo, Tokyo, Japan

*Contributed equally.

The authors declare no conflicts of interest.

0022-3476/$ - see front matter. http://dx.doi.org/10.1016/j.jpeds.2013.01.003

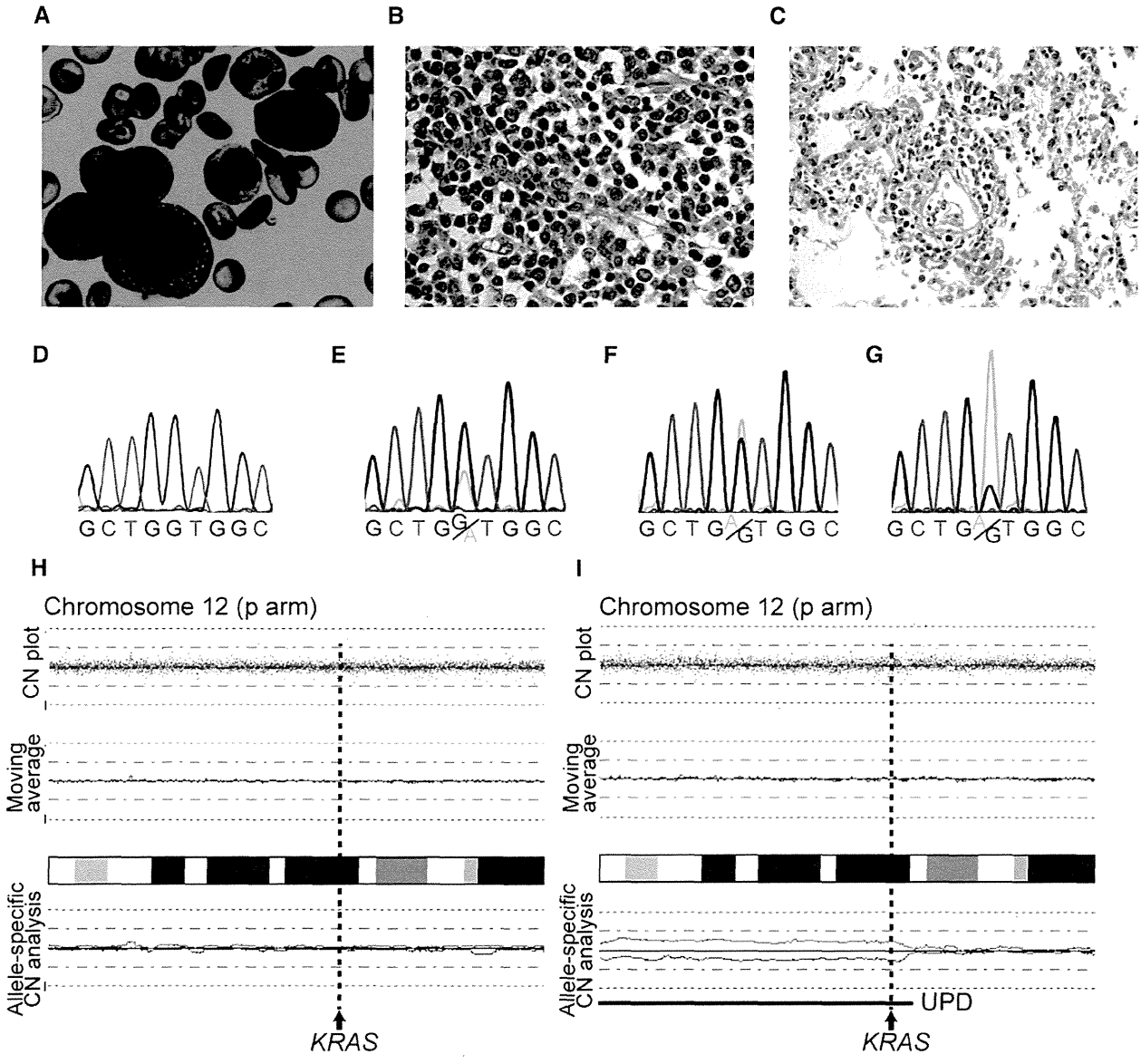

Figure 1. Blood smear, autopsy, and genomic analysis results. **A,** May-Giemsa staining of peripheral blood at progression. Hematoxylin & eosin staining of **B,** bone marrow and **C,** lung. Results of direct sequencing for the *KRAS* gene in **D,** heart, **E,** muscle, **F,** peripheral blood at diagnosis, and **G,** peripheral blood at progression. Results of SNP array analysis for PBMCs at **H,** diagnosis and **I,** progression. UPD at the 12p locus was detected at progression (*brown line*), whereas UPD was absent at diagnosis. Total copy number plots from each probe (*red points*) and moving average (n = 20; *blue line*) are shown *above* the cytoband. Results from allele-specific analyses are given *below* the cytoband. The larger allele is presented in *red*; the smaller allele, in *blue*. *CN*, copy number.

extracted from samples was analyzed using the GeneChip Human Mapping 250K *NspI* array (Affymetrix, Santa Clara, California). The data thus obtained were processed using CNAG/AsCNAR software (http://www.genome.umin.jp).[5,6]

Results and Discussion

This case shows that JMML can progress rapidly during an indolent clinical course, with invasion into multiple organs. The aggressive transformation of JMML is similar to that of blast crisis in chronic myelogenous leukemia but is rare,[2,3] and the definition and molecular biology of the blast crisis–like aggressive transformation of JMML remain unclear.

Direct sequencing of the *KRAS* gene revealed a mutation in normal muscle. The same mutation was found in the lung, but not in the heart. The mutation was also detected in PBMCs at diagnosis, and the mutation became homozygous in PBMCs at progression (Figure 1, D-G). SNP array analysis

detected uniparental disomy (UPD) at the 12p locus, which included the *KRAS* gene, in PBMCs at progression (Figure 1, I). The UPD was absent in PBMCs at diagnosis (Figure 1, H). Our genome-wide analysis for copy number alteration and allelic imbalances using high-density SNP arrays detected no other genetic abnormalities in samples, either at diagnosis or at progression.

Recent research identified germline/somatic mutations in genes regulating the Ras-MAPK pathway as responsible for JMML pathogenesis, but the underlying mechanism of aggressive transformation remains unclear. Reportedly, abrogation of the wild-type *NRAS* allele was evident at progression, similar to our results.[7] Loss of the remaining *KRAS* allele could be associated with JMML progression because the wild-type *KRAS* allele functions as a tumor suppressor.[8] However, we determined that UPD at the 12p locus occurred at progression, leading to both a loss of the remaining allele and an increase in the dosage of the mutant *KRAS* allele. Previous studies have found strong associations between UPD at oncogene loci and the onset of various hematologic neoplasms, such as *NRAS* in chronic myelomonocytic leukemia[9,10] and *CBL* in adult myelodysplastic syndrome.[11] Our analysis suggested that UPD of mutant *KRAS* contributed to aggressive transformation as a second hit in our patient, leading to increased aberrant activation of the Ras-MAPK pathway (Figure 3).

Our patient received oral 6-MP for disease stabilization before progression. Of note, 6-MP has a DNA-damaging effect. A previous report suggested a correlation between 6-MP maintenance therapy and secondary malignant neoplasms.[12] Although an association between 6-MP and progression is unelucidated, it is possible that 6-MP might induce the second hit, followed by progression to cell transformation.

We found no genomic lesions other than the *KRAS* mutation in samples obtained at diagnosis, and the first hit for JMML onset remains undetermined. Previous reports have identified other genetic and epigenetic abnormalities were associated with JMML pathogenesis, including mutation of *TP53* and methylation of *BMP4*, *CALCA*, *CDKN2B*, and *RARB*.[13] However, direct sequencing of *TP53* and methylation-specific polymerase chain reaction showed that *BMP4* and *RARB* were not methylated and *CALCA* was methylated both at diagnosis and at progression, and *CDKN2B* was partially methylated only at progression. Further research is needed to elucidate the etiology of JMML.

In our patient, we detected *KRAS* G13D mutation in normal muscle cells in which we pathologically excluded blood infiltration. However, we found no facial gestalt or developmental retardation characteristic of Noonan or cardio-facio-cutaneous syndromes, both of which are caused by germline *KRAS* mutations. We assumed that this is because the patient was mosaic for a *KRAS* mutation, supported by sequencing results using other normal cells (Figure 1, D and E). Here we report a patient with JMML and oncogenic *KRAS* mosaicism who developed JMML. In another report of 2 cases of *NRAS* mosaic mutation with JMML, *NRAS* mutations remained heterozygous, and both patients exhibited an indolent clinical course.[14]

It is accepted that most patients with JMML harboring a *KRAS* mutation experience an indolent clinical course, and some achieve spontaneous remission.[1,15] However, as we report here, some patients with JMML with a *KRAS* mutation experience aggressive transformation, which is potentially fatal. We suggest that UPD at the mutated *KRAS* gene causes more potent activation of the Ras-MAPK pathway, facilitating transformation. Consequently, inhibition of this pathway could be a therapeutic target for JMML. ■

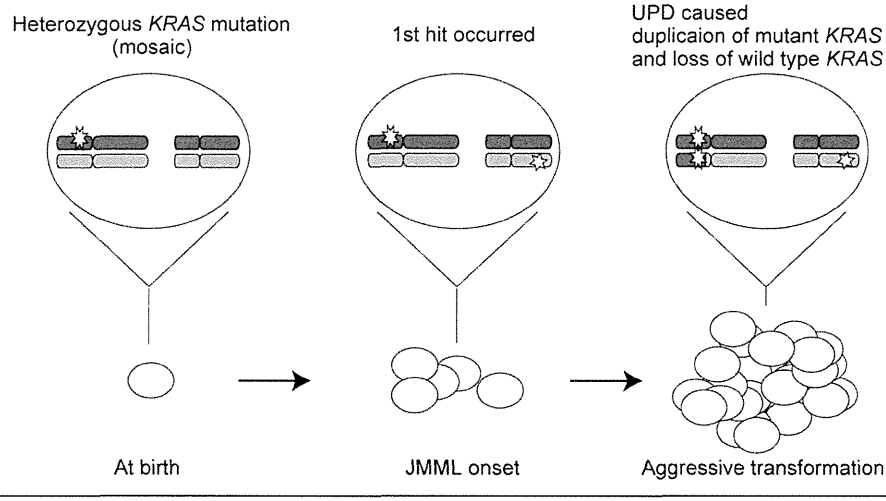

Figure 3. Hypothetical model of onset of JMML and its aggressive transformation. Sequential genetic events, starting with the presence of a *KRAS* mutation, are indicated. A first hit contributed to JMML onset, although that first hit remains undetermined. *KRAS*-mutated cells acquired UPD at the 12p locus, leading to both a loss of the wild-type *KRAS* allele and an increase in the dosage of the mutant *KRAS* allele, followed by aggressive transformation.

Submitted for publication Aug 16, 2012; last revision received Nov 16, 2012; accepted Jan 2, 2013.

Reprint requests: Motohiro Kato, Department of Hematology/Oncology, Saitama Children's Medical Center, 2100 Magome, Iwatsuki-ku, Saitama 339-8551, Japan. E-mail: katom-tky@umin.ac.jp

References

1. Loh ML. Recent advances in the pathogenesis and treatment of juvenile myelomonocytic leukaemia. Br J Haematol 2011;152:677-87.
2. Niemeyer CM, Arico M, Basso G, Biondi A, Cantu Rajnoldi A, Creutzig U, et al., European Working Group on Myelodysplastic Syndromes in Childhood (EWOG-MDS). Chronic myelomonocytic leukemia in childhood: a retrospective analysis of 110 cases. Blood 1997;89:3534-43.
3. Luna-Fineman S, Shannon KM, Atwater SK, Davis J, Masterson M, Ortega J, et al. Myelodysplastic and myeloproliferative disorders of childhood: a study of 167 patients. Blood 1999;93:459-66.
4. Chan RJ, Cooper T, Kratz CP, Weiss B, Loh ML. Juvenile myelomonocytic leukemia: a report from the 2nd International JMML Symposium. Leuk Res 2009;33:355-62.
5. Nannya Y, Sanada M, Nakazaki K, Hosoya N, Wang L, Hangaishi A, et al. A robust algorithm for copy number detection using high-density oligonucleotide single nucleotide polymorphism genotyping arrays. Cancer Res 2005;65:6071-9.
6. Yamamoto G, Nannya Y, Kato M, Sanada M, Levine RL, Kawamata N, et al. Highly sensitive method for genomewide detection of allelic composition in nonpaired, primary tumor specimens by use of Affymetrix single-nucleotide polymorphism genotyping microarrays. Am J Hum Genet 2007;81:114-26.
7. Matsuda K, Nakazawa Y, Sakashita K, Shiohara M, Yamauchi K, Koike K. Acquisition of loss of the wild-type NRAS locus with aggressive disease progression in a patient with juvenile myelomonocytic leukemia and a heterozygous NRAS mutation. Haematologica 2007;92:1576-8.
8. Zhang Z, Wang Y, Vikis HG, Johnson L, Liu G, Li J, et al. Wild-type Kras2 can inhibit lung carcinogenesis in mice. Nat Genet 2001;29:25-33.
9. Dunbar AJ, Gondek LP, O'Keefe CL, Makishima H, Rataul MS, Szpurka H, et al. 250K single nucleotide polymorphism array karyotyping identifies acquired uniparental disomy and homozygous mutations, including novel missense substitutions of c-Cbl, in myeloid malignancies. Cancer Res 2008;68:10349-57.
10. Wang J, Liu Y, Li Z, Du J, Ryu MJ, Taylor PR, et al. Endogenous oncogenic Nras mutation promotes aberrant GM-CSF signaling in granulocytic/monocytic precursors in a murine model of chronic myelomonocytic leukemia. Blood 2010;116:5991-6002.
11. Sanada M, Suzuki T, Shih LY, Otsu M, Kato M, Yamazaki S, et al. Gain-of-function of mutated C-CBL tumour suppressor in myeloid neoplasms. Nature 2009;460:904-8.
12. Schmiegelow K, Al-Modhwahi I, Andersen MK, Behrendtz M, Forestier E, Hasle H, et al. Methotrexate/6-mercaptopurine maintenance therapy influences the risk of a second malignant neoplasm after childhood acute lymphoblastic leukemia: results from the NOPHO ALL-92 study. Blood 2009;113:6077-84.
13. Olk-Batz C, Poetsch AR, Nollke P, Claus R, Zucknick M, Sandrock I, et al. Aberrant DNA methylation characterizes juvenile myelomonocytic leukemia with poor outcome. Blood 2011;117:4871-80.
14. Doisaki S, Muramatsu H, Shimada A, Takahashi Y, Mori-Ezaki M, Sato M, et al. Somatic mosaicism for oncogenic *NRAS* mutations in juvenile myelomonocytic leukemia. Blood 2012;120:1485-8.
15. Matsuda K, Shimada A, Yoshida N, Ogawa A, Watanabe A, Yajima S, et al. Spontaneous improvement of hematologic abnormalities in patients having juvenile myelomonocytic leukemia with specific RAS mutations. Blood 2007;109:5477-80.

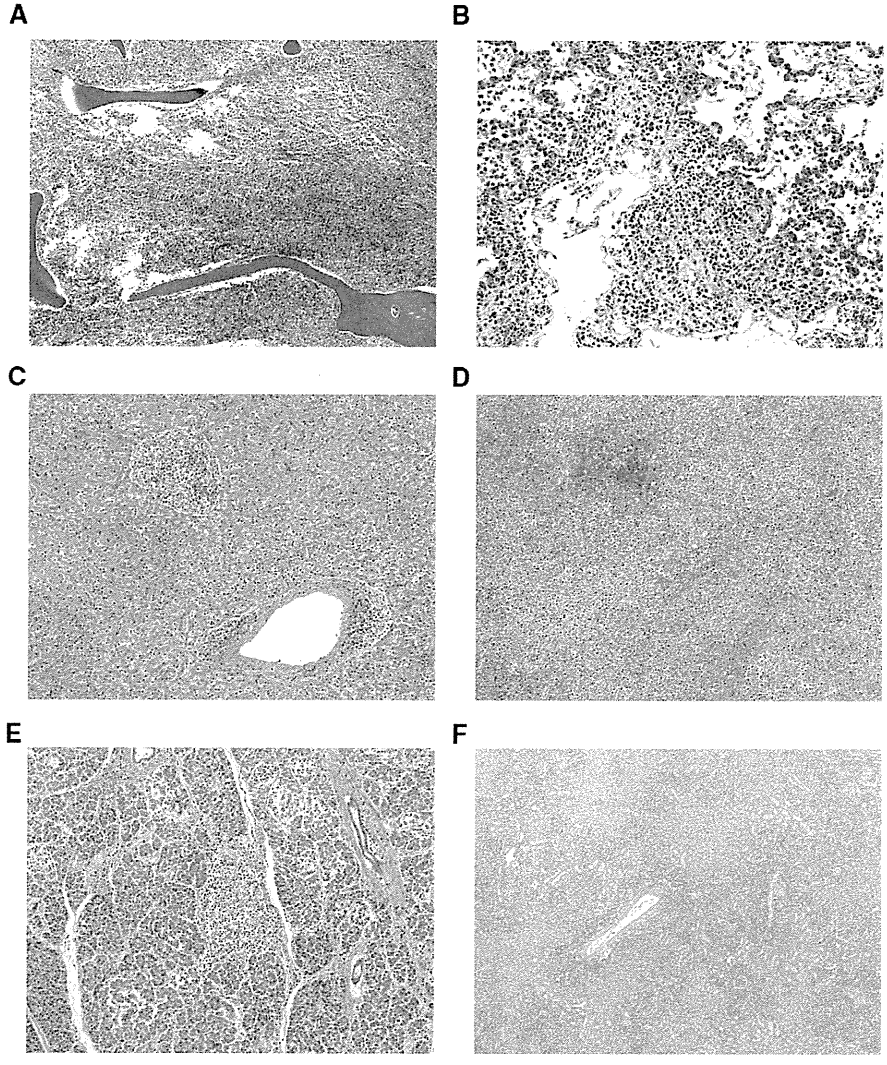

Figure 2. Autopsy revealed dysplastic cells infiltrated into mutiple organs. Hematoxylin & eosin staining of **A,** bone marrow; **B,** lung; **C,** liver; **D,** spleen; **E,** pancreas; and **F,** kidney.

Bone Marrow Transplantation (2013) **48,** 312–313

www.nature.com/bmt

LETTER TO THE EDITOR

Successful syngeneic PBSC transplantation for a patient with refractory Evans syndrome

Bone Marrow Transplantation (2013) **48,** 312–313; doi:10.1038/bmt.2012.136; published online 16 July 2012

Evans syndrome (ES) is a haematological disorder characterised by the simultaneous or sequential development of autoimmune thrombocytopenia (AITP) and autoimmune haemolytic anaemia (AIHA). Haematopoietic SCT (HSCT) is an effective treatment for autoimmune cytopenias such as AITP, AIHA and ES. In patients who are successfully treated, self-reacting lymphocyte clones could be eliminated or inhibited with myeloablative conditioning and/or through the graft versus autoimmunity (GVA) effect, such that a cure or long-term remission is reasonably expected at the cost of the toxicity associated with HSCT.[1]

A 10-year-old boy was diagnosed with AIHA in November 2004. Although he responded to corticosteroid (CS), repeated recurrence was observed when the CS dose was tapered off. Fluctuating thrombocytopenia was identified in September 2006, and thus a diagnosis of ES was made. No underlying disease including autoimmune lymphoproliferative syndrome (ALPS) was identified.[2]

While fluctuating, the number of thrombocytes would sometimes fall to 1×10^9/L or less. Intracranial haemorrhage, severe epistaxis and buccal bleeding occurred during the clinical course. Although multiple therapeutic options that are reportedly effective for the treatment of ES, including high-dose intravenous immunoglobulin infusion (IVIG), CsA, rituximab, cepharanthine, vincristine, mycophenolate mofetil, 6-mercaptopurine, dapsone, danazol, and high-dose CY together with splenectomy and accessory splenectomy, had been used since the onset of ES, the results were unsatisfactory (Figure 1).

Among the treatments, the patient had been given prednisolone and CsA for 6 and 2 years, respectively, at variable doses. He had a Cushingoid appearance, short stature, acne and verrucae on the skin, a compression fracture of a lumbar vertebra, chronic intermittent headache, stiffness of the muscles, insomnia, lymphocytopenia and osteoporosis, which were thought to be adverse effects due to one of these two agents.

As the patient has an identical twin brother, a syngeneic HSCT was planned because no other treatment modality was considered promising. Withdrawal from CS and CsA, which had been given for an extended period, was also thought to be desirable. The donor-to-be brother was completely healthy with no evidence of ALPS. The suggestion of syngeneic HSCT was made to the patient, the parents and the brother, and written consent from the family was obtained.

The conditioning regimen consisted of CY at a dose of 50 mg/kg/day i.v. infusion from day −4 to −1 before the transplant. The donor was given G-CSF for mobilisation. A total of 7.7×10^8/kg of unmanipulated PBMC (3.8×10^6/kg of CD34-positive cells) was harvested and infused into the patient in October 2010.

Neutrophil recovery (0.5×10^9/L) was identified on day 10. The patient's platelet level reached a normal level on day 180. His platelet count and Hb level at 8 months post transplantation were 17.3×10^9/L and 14.7 g/dL, respectively. The patient remains in remission without therapy 17 months after the syngeneic PBSCT, the longest remission period ever experienced by this patient (Figure 1). Of note, although the levels of haptoglobin, indirect bilirubin, aspartate transaminase, lactate dehydrogenase and reticulocytes are normal, the direct Coombs test remains positive up to day 582, suggesting that minimal autoantibody is being produced by long-lived plasma cells with limited extravascular haemolysis due to splenectomy and accessory splenectomy. In this case, however, the patient is still deemed to be in CR by the definition of Passweg.[1]

We surveyed the literature and identified 18 reports detailing a total of 23 patients with ES treated with 26 HSCTs. The definitions of CR, relapse (REL) and treatment-related mortality (TRM) used herein are defined using the definitions of Passweg.[1] The median age of the patients who underwent HSCT is 21 years. The median time course from the onset of the disease to HSCT is 5.42 years, and a median of seven treatment modalities were used before HSCT. Of the 26 HSCTs, 15 were autologous and 11 were allogeneic. CD34-positive cell selection was employed in all of the autologous HSCTs except for 2, for which the details were not described. The results were compared between autologous and allogeneic HSCTs (Table 1). More patients who underwent allogeneic HSCT likely achieved CR than patients who underwent autologous HSCT at the cost of therapeutic toxicity: CR was attained in 4 out of 15 autologous transplantations and in 8 out of 11 allogeneic transplantations. REL occurred in 5 out of 15 patients who underwent autologous transplantation. A list of information on patients and HSCTs collected here and organised in a table can be provided upon request.

We reasoned that HSCT is indicated for those cases with ES (i) when continued immunosuppressive intervention reduced the quality of life of the patients and (ii) when the disease activity is not satisfactorily controlled with the conventional therapy described herein or elsewhere.[3] The indications for HSCT in the present case are in line with the current EBMT autoimmune diseases working party guidelines, which describe the indications for HSCT as a treatment for immune cytopenia, paediatric cases and syngeneic transplantation.[4]

Recently, TPO receptor antagonists have become a promising treatment option for chronic AITP. The indications for HSCT for the treatment of ES could therefore be revised if TPO receptor antagonists are demonstrated to be effective for the control of thrombocytopenia in patients with ES. However, future evaluations are required to determine the long-term therapeutic significance of these drugs.

A syngeneic immune system has been reported to cause a graft versus host reaction, possibly due to post-somatic modification.[5] Studies comparing the T-cell repertoire before and after the transplantation could have scientific significance. A prospective study and material banking should provide some information on the possible effects of GVA in syngeneic transplantation.

Zayden *et al.*[6] reported effective syngeneic PBSCT for a case of chronic ITP. They employed reduced myeloablative conditioning with CY and TBI. The patient had been in CR for 12 months after the syngeneic HSCT without any transplantation-related toxicity. Their experience and ours suggests that when available, a syngeneic transplant could be the preferred treatment if the expected outcomes of conventional therapies are sufficiently

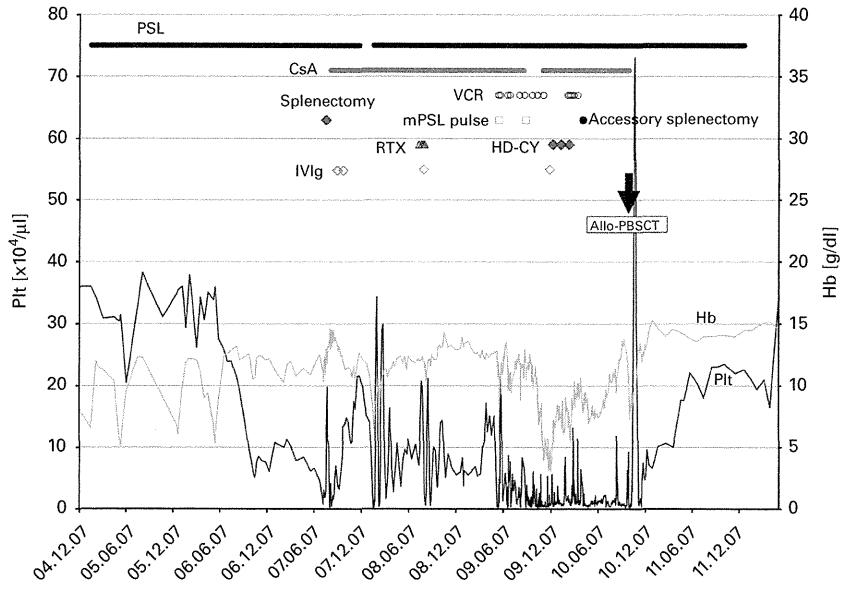

Figure 1. The time course of platelet count, the Hb level and the selected treatments that were at least partially or transiently effective. Black line, platelet number ($\times 10^4$/mm^3, left axis); grey line, Hb level (g/dL, right axis). PSL = prednisolone; VCR = vincristine; mPSL pulse = methylprednisolone pulse therapy; IVIg = high-dose gammaglobulin; RTX = rituximab; allo-PBSCT = allogeneic PBSCT. Note that PSL had been given for physiological replacement after transplantation due to steroid therapy for an extended period.

Table 1. Outcomes of the patients treated with HSCT

	Autologous	*Allogeneic*
CR/PR	4	7
NR	4	0
REL	5	1
TRM	1	3
IE	1	0
Total	15	11

Abbreviations: HSCT = haematopoietic SCT; IE = inevaluable; NR = no response; REL = relapse; TRM = treatment-related mortality.

limited to justify the expected adverse effect of HSCT. Although the clinical course of our patient after the transplant is uneventful thus far, careful observation is definitely necessary because a REL of ES 5 years after allogeneic transplant despite full donor chimerism is reported.[7]

CONFLICT OF INTEREST

The authors declare no conflict of interest.

M Mori[1,2], M Hiwatari[3], J Takita[4], K Ida[3] and H Kawaguchi[2,5]
[1]Department of Haematology/Oncology, Saitama Children's Medical Center, Saitama, Japan;
[2]Department of Paediatrics, Tokyo Dental College Ichikawa General Hospital, Chiba, Japan;
[3]Department of Paediatrics, University of Tokyo Hospital, Tokyo, Japan;
[4]Department of Cell Therapy and Transplantation Medicine, University of Tokyo Hospital, Tokyo, Japan and
[5]Department of Paediatrics, National Defense Medical College, Saitama, Japan
E-mail: hiroyuki.kawaguchi@gmail.com

REFERENCES

1 Passweg JR, Rabusin M. Hematopoetic stem cell transplantation for immune thrombocytopenia and other refractory cytopenias. *Autoimmunity* 2008; **41**: 660–665.
2 Seif AE, Manno CS, Sheen C, Grupp SA, Teachey DT. Identifying autoimmune lymphoproliferative syndrome in children with Evans syndrome: a multi-institutional study. *Blood* 2010; **115**: 2142–5214.
3 Michel M, Chanet V, Dechartres A, Morin AS, Piette JC, Cirasino L *et al.* The spectrum of Evans syndrome in adults: new insight into the disease based on the analysis of 68 cases. *Blood* 2009; **114**: 3167–3172.
4 Snowden JA, Saccardi R, Allez M, Ardizzone S, Arnold R, Cervera R *et al.* Haematopoietic SCT in severe autoimmune diseases: updated guidelines of the European Group for Blood and Marrow Transplantation. *Bone Marrow Transplant* 2011; **47**: 770–790.
5 McColl G, Kohsaka H, Szer J, Wicks I. High-dose chemotherapy and syngeneic hemopoietic stem-cell transplantation for severe, seronegative rheumatoid arthritis. *Ann Intern Med* 1999; **131**: 507–509.
6 Zaydan M, Turner C, Miller A. Resolution of chronic idiopathic thrombocytopenia purpura following syngeneic peripheral blood progenitor transplant. *Bone Marrow Transplant* 2002; **29**: 87–89.
7 Marmont AM, Gualandi F, Occhini D, Morandi F, Ferretti E, Pezzolo A *et al.* Catastrophic relapse of Evans syndrome five years after allogeneic BMT notwithstanding full donor chimerism. Terminal hemolytic-uremic syndrome. *Autoimmunity* 2006; **39**: 505–511.

CBL mutations in infant acute lymphoblastic leukaemia

Infant acute lymphoblastic leukaemia (ALL) is relatively rare, occurring in approximately 2·5–5% of cases of childhood ALL (Biondi *et al*, 2000). Infant ALLs are much more likely to present with high leucocyte counts, hepatosplenomegaly and overt central nervous system (CNS) diseases (Taki *et al*, 1996). T cell phenotype is much less common in infants, while myeloid antigen co-expression and the absence of CD10 expression are more frequent in infants than in older children with ALL. When molecular techniques [such as fluorescence *in situ* hybridization (FISH) or Southern blot analysis] are used in addition to karyotype, *MLL* gene rearrangements (*MLL*-R) are found in 70–80% of infant ALL compared with only 2–4% of older children with ALL (Taki *et al*, 1996; Biondi *et al*, 2000). Thus, infant ALL appears to be biologically distinct from the disease in older children (more than 1 year old).

In this regard, recent reports of somatic mutations of the *CBL* proto-oncogene in myeloid neoplasms are intriguing, because these *CBL* mutations were shown to result in aberrant tyrosine kinase signalling, which also leads to activation of RAS signalling pathways. So far, we and others have reported that *CBL* mutations occur in a variety of myeloid neoplasms, including *de novo* acute myeloid leukaemia (AML) (Caligiuri *et al*, 2007), myelodysplastic syndrome (MDS), and myeloproliferative neoplasm, especially in chronic myelomonocytic leukaemia (CMML) (Sanada *et al*, 2009), and juvenile myelomonocytic leukaemia (JMML) (Shiba *et al*, 2010). The importance of *CBL* mutations regarding leukaemogenesis is substantially increased. Recently, we found *CBL* mutation in therapy-related AML with *MLL*-R (Shiba *et al*, 2011). Interestingly, the *MLL-CBL* fusion gene has been reported in a *de novo* AML case (Fu *et al*, 2003), and this prompted us to search for possible *CBL* mutations in infant ALL with *MLL-R*.

Because *CBL* mutations thus far reported were almost all clustered within exons 8–9 that encode Linker/RING finger domains (Caligiuri *et al*, 2007; Sanada *et al*, 2009; Shiba *et al*, 2010), we confined our mutation analysis to these exons, in which polymerase chain reaction-amplified exons 8–9 were subjected to direct sequencing using an ABI PRISM 310 Genetic Analyser (Applied Biosystems, Branchburg, NJ, USA). The study adhered to the principles of the Helsinki Declaration, and was conducted under the regulations enacted by the Ethics Board of Gunma Children's Medical Centre.

CBL gene analysis was performed in 41 infant ALL patients in which *MLL*-R was found in 33 patients (80·5%), including 15 patients with t(4;11)(q21;q23), 4 with t(9;11)(p22;q23) and 5 with t(11;19)(q23;p13.3). Median age at diagnosis was 4·7 months (range, 0–12 months). We also performed *CBL* gene mutation analysis in 28 B cell precursor (BCP)-ALL patients (age range, 1–14 years).

Heterozygous mutations of the *CBL* gene were identified in 2 (4·9%) of 41 infant ALL patients, but not in older children with BCP-ALL. These were located in exon 8 (Fig 1). One patient was a 3-month-old female with t(4;11)(q21;q23) and the other patient was a 6-month-old male with t(11;19)(q23;p13.3). They were registered and treated on two Japanese infant leukaemia protocols, MLL96 and MLL98 respectively (Isoyama *et al*, 2002; Kosaka *et al*, 2004). Although strong association between *CBL* mutations and 11q-acquired uniparental disomy (aUPD) has been reported (Sanada *et al*, 2009), we did not perform the single nucleotide polymorphism array analysis due to lack of DNA.

MLL-R are more frequent in younger infants; up to 90% of infant ALL less than 6 months old at diagnosis have detectable *MLL*-R compared with 30–50% of infant ALL aged 6–12 months (Taki *et al*, 1996). *MLL*-R ALL has a characteristic gene expression profile that significantly differs from that of non-*MLL*-R BCP-ALL and of AML, confirming that *MLL*-R ALL is a biologically unique leukaemia subtype.

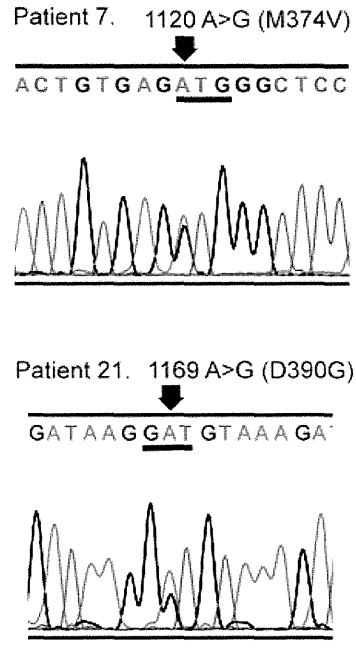

Fig 1. Identification of *CBL* mutations. Heterozygous mutations of the *CBL* gene were identified in Patients 7 and 21.

Thus, the distinctive presenting features and clinical behaviour of infant ALL appear to be primarily due to the high frequency of *MLL*-R in this age group. However, outcome data comparing infant and non-infant patients with *MLL*-R suggest that there may be other factors which impact the prognosis of infant ALL. Both of the patients with *CBL* mutations were diagnosed before 6 months of age. In our previous report, all of three cases with *CBL* mutation developed JMML before 4 months of age (Shiba *et al*, 2010). These data suggested that *CBL* mutation may have a strong association with very early onset disease. *CBL* mutations have been reported as germline mutations in JMML (Niemeyer *et al*, 2010). Unfortunately, we could not investigate whether the mutations in our cases were germline mutations or not, because somatic cells were not available.

CBL mutations have been found in approximately 5% of 2000 samples from patients with myeloid neoplasms, including AML transformed from MDS. Gene aberrations in addition to *MLL*-R have rarely been reported in infant ALL. No reports of ALL with *CBL* mutations have so far been reported, suggesting that the pathogenesis of infant ALL is different from paediatric or adult ALL. To our knowledge, this is the first report of infant ALL patients with 11q23 translocation/*MLL*-R and *CBL* mutations. The present study suggests that alterations of *CBL* gene and *MLL*-R may cooperatively play a pathogenic role in the development of infant ALL with *MLL*-R.

Acknowledgements

We thank Mrs. Chisato Murata for her excellent technical assistance. This work was supported by a grant for Cancer Research, and a grant for Research on Children and Families from the Ministry of Health, Labour, and Welfare of Japan, a Grant-in-Aid for Scientific Research (B, C) and Exploratory Research from the Ministry of Education, Culture, Sports, Science, and Technology of Japan and by a Research grant for Gunma Prefectural Hospitals.

Author's contributions

TT and YH designed the study. JT, MH, TK, MS and EI provided critical reagents and samples. NS and MP performed the experiments. EI, HA and SO supervised the work. NS and MP analysed the results. NS, TT, and YH wrote the paper and all the authors critically reviewed and revised it.

Conflict of interest

The authors declare no conflict of interest.

Norio Shiba[1,2]
Myoung-Ja Park[1]
Tomohiko Taki[3]
Junko Takita[4]
Mitsuteru Hiwatari[4]
Takashi Kanazawa[2]
Manabu Sotomatsu[1]
Eiichi Ishii[5]
Hirokazu Arakawa[2]
Seishi Ogawa[6]
Yasuhide Hayashi[1]

[1]Department of Haematology/Oncology, Gunma Children's Medical Centre, [2]Department of Paediatrics, Gunma University Graduate School of Medicine, Gunma, [3]Department of Molecular Diagnostics and Therapeutics, Kyoto Prefectural University of Medicine Graduate School of Medical Science, Kyoto, [4]Department of Paediatrics, Graduate School of Medicine, University of Tokyo, Tokyo, [5]Department of Paediatrics, Ehime University Graduate School of Medicine, Ehime, and [6]Cancer Genomics Project, Graduate School of Medicine, University of Tokyo, Tokyo, Japan.
E-mail: hayashiy-tky@umin.ac.jp

Keywords: infant, ALL, *MLL*, *CBL*.

First published online 11 October 2011
doi: 10.1111/j.1365-2141.2011.08900.x

References

Biondi, A., Cimino, G., Pieters, R. & Pui, C.H. (2000) Biological and therapeutic aspects of infant leukemia. *Blood*, **96,** 24–33.

Caligiuri, M.A., Briesewitz, R., Yu, J., Wang, L., Wei, M., Arnoczky, K.J., Marburger, T.B., Wen, J., Perrotti, D., Bloomfield, C.D. & Whitman, S.P. (2007) Novel c-CBL and CBL-b ubiquitin ligase mutations in human acute myeloid leukemia. *Blood*, **110,** 1022–1024.

Fu, J.F., Hsu, J.J., Tang, T.C. & Shih, L.Y. (2003) Identification of CBL, a protooncogene at 11q23.3, as a novel MLL fusion partner in a patient with de novo acute myeloid leukemia. *Genes Chromosomes Cancer*, **37,** 214–219.

Isoyama, K., Eguchi, M., Hibi, S., Kinukawa, N., Ohkawa, H., Kawasaki, H., Kosaka, Y., Oda, T., Oda, M., Okamura, T., Nishimura, S., Hayashi, Y., Mori, T., Imaizumi, M., Mizutani, S., Tsukimoto, I., Kamada, N. & Ishii, E. (2002) Risk-directed treatment of infant acute lymphoblastic leukaemia based on early assessment of MLL gene status: results of the Japan Infant Leukaemia Study (MLL96). *British Journal of Haematology*, **118,** 999–1010.

Kosaka, Y., Koh, K., Kinukawa, N., Wakazono, Y., Isoyama, K., Oda, T., Hayashi, Y., Ohta, S., Moritake, H., Oda, M., Nagatoshi, Y., Kigasawa, H., Ishida, Y., Ohara, A., Hanada, R., Sako, M., Sato, T., Mizutani, S., Horibe, K. & Ishii, E. (2004) Infant acute lymphoblastic leukemia with MLL gene rearrangements: outcome following intensive chemotherapy and hematopoietic stem cell transplantation. *Blood*, **104,** 3527–3534.

Niemeyer, C.M., Kang, M.W., Shin, D.H., Furlan, I., Erlacher, M., Bunin, N.J., Bunda, S., Finklestein, J.Z., Sakamoto, K.M., Gorr, T.A., Mehta, P., Schmid, I., Kropshofer, G., Corbacioglu, S., Lang, P.J., Klein, C., Schlegel, P.G., Heinzmann, A., Schneider, M., Starý, J., van, den., Heuvel-Eibrink, M.M., Hasle, H., Locatelli, F., Sakai, D., Archambeault, S., Chen, L., Russell, R.C., Sybingco, S.S., Ohh, M., Braun, B.S., Flotho, C. & Loh, M.L. (2010) Germline CBL mutations cause developmental abnormalities and predispose to juvenile myelomonocytic leukemia. *Nature Genetics*, **42,** 794–800.

Sanada, M., Suzuki, T., Shih, L.Y., Otsu, M., Kato, M., Yamazaki, S., Tamura, A., Honda, H., Sakata-Yanagimoto, M., Kumano, K., Oda, H., Yamagata, T., Takita, J., Gotoh, N., Nakazaki, K., Kawamata, N., Onodera, M., Nobuyoshi, M.,

Hayashi, Y., Harada, H., Kurokawa, M., Chiba, S., Mori, H., Ozawa, K., Omine, M., Hirai, H., Nakauchi, H., Koeffler, H.P. & Ogawa, S. (2009) Gain-of-function of mutated C-CBL tumour suppressor in myeloid neoplasms. *Nature*, **460,** 904–908.

Shiba, N., Kato, M., Park, M.J., Sanada, M., Ito, E., Fukushima, K., Sako, M., Arakawa, H., Ogawa, S. & Hayashi, Y.. (2010) CBL mutations in juvenile myelomonocytic leukemia and pediatric myelodysplastic syndrome. *Leukemia*, **24,** 1090–1092.

Shiba, N., Taki, T., Park, M.J., Nagasawa, M., Kanazawa, T., Takita, J., Ohnishi, H., Sotomatsu, M., Arakawa, H. & Hayashi, Y. (2011) CBL mutation in childhood therapy-related leukemia. *Leukemia*, **25,** 1356–1358.

Taki, T., Ida, K., Bessho, F., Hanada, R., Kikuchi, A., Yamamoto, K., Sako, M., Tsuchida, M., Seto, M., Ueda, R. & Hayashi, Y. (1996) Frequency and clinical significance of the MLL gene rearrangements in infant acute leukemia. *Leukemia*, **10,** 1303–1307.

MCB
Journals.ASM.org

HuR Maintains a Replicative Life Span by Repressing the ARF Tumor Suppressor

Hiroyuki Kawagishi,[a]* Michihiro Hashimoto,[a] Hideaki Nakamura,[a] Takayuki Tsugawa,[a] Atsushi Watanabe,[a] Dimitris L. Kontoyiannis,[b] Masataka Sugimoto[a]

Research Institute, National Center for Geriatrics and Gerontology, Obu, Aichi, Japan[a]; Institute of Immunology, Alexander Fleming Biomedical Science Research Center, Vari, Greece[b]

$p19^{ARF}$ plays an essential role in the senescence of mouse cells, and its expression is lost by methylation or deletion of the *ARF* locus; otherwise, p53 is inactivated to bypass senescence. *ARF* expression is tightly regulated, but little is known about its post-transcriptional regulation. Here, we show that an RNA-binding protein, HuR (human antigen R), represses *ARF* mRNA translation, thereby maintaining the replicative life span of mouse embryonic fibroblasts (MEFs). Loss of HuR results in premature senescence, with concomitant increases in $p19^{ARF}$ but not $p16^{Ink4a}$ levels, and this senescence is not observed in *ARF*-null MEFs that retain an intact *Ink4a* locus. HuR depletion does not alter *ARF* transcription or stability but enhances ribosome association with *ARF* mRNA. Under these conditions, *ARF* mRNA accumulates in nucleoli, where it associates with nucleolin. Furthermore, adipose-specific deletion of the *HuR* gene results in increased $p19^{ARF}$ expression in aged animals, which is accompanied by decreased insulin sensitivity. Together, our findings demonstrate that $p19^{ARF}$ is also regulated at the translational level, and this translational regulation restrains the cellular life span and tissue functions *in vivo*.

Most mammalian somatic cells have a limited replicative life span when cultured *in vitro* and eventually undergo irreversible growth arrest, called cellular senescence (1). Senescence is caused by excessive extracellular or intracellular stress, and senescent cells are observed in tissues of aged animals and in tissues that experience prolonged inflammation (2, 3). Two major tumor suppressor pathways, the $p19^{ARF}$ ($p14^{ARF}$ in humans)-p53 and $p16^{Ink4a}$-retinoblastoma (Rb) pathways, play critical roles in inducing and maintaining permanent cell cycle arrest during cellular senescence (4, 5), and inactivation of these proteins bypasses cellular senescence, allowing damaged cells to survive and proliferate. Thus, senescence prevents the spread of damaged cells, eliminating potential malignant transformation, and acts as a potent tumor-suppressive mechanism in mammals (6, 7).

Human antigen R (HuR) is a ubiquitously expressed member of the ELAV/Hu protein family and is involved in diverse biological processes (8, 9). Loss of HuR causes midgestational embryonic lethality due to placental defects (10). Animals rescued from this defect can develop to later stages but mostly die by embryonic day 19.5 and exhibit prominent defects in skeletal and splenic development. *HuR* encodes an RNA-binding protein that controls the stability, translation, splicing, and intracellular localization of its target mRNA (11, 12). Canonically, HuR directly binds to AU-rich elements (ARE) in the 3′ untranslated region (3′UTR) of its target mRNA, and the biological consequence of HuR association varies depending on the mRNA to which it binds (13, 14). In most cases, HuR stabilizes the mRNA associated with it; for instance, HuR has been shown to stabilize *VEGF*, β-*actin*, *DNMT3b*, and *TNF*-α mRNA (15–18). The mechanisms by which HuR regulates mRNA stability are not fully understood, but competition with other ARE-binding proteins is likely to be involved (19). Additionally, HuR is involved in microRNA (miRNA) recruitment to target mRNA. In this case, binding of HuR adjacent to the let-7 binding site on c-*Myc* mRNA facilitates the recruitment of let-7-loaded miRNA-induced silencing complexes (RISC) (20). Conversely, HuR has been shown to compete with miR-494 on *Nucleolin* mRNA (21).

It has become evident that HuR controls replicative senescence in human diploid fibroblasts (HDFs) (22). HuR levels decline during senescence in HDFs and are low in aged human tissues, and miR-519 is responsible for the downregulation of HuR in senescent HDFs (23, 24). HuR destabilizes *Ink4a* mRNA, the encoded protein of which, $p16^{Ink4a}$, plays an important role in the cellular senescence of HDFs. HuR recruits RISC to *Ink4a* mRNA, and this process does not require miRNA but is mediated by the direct interaction of RISC with HuR proteins on mRNA (25). Additionally, HuR controls the mRNA metabolism of other senescence-related genes, including *p53*, *p21*, and *cyclin D1*, in response to cellular stress, such as UV (19, 26, 27). Therefore, HuR likely participates in cellular senescence by organizing the expression of multiple genes.

While the involvement of HuR in human cellular senescence has been documented, little is known about the function of HuR in the replicative senescence of mouse cells. Unlike in human cells, where the Ink4a-Rb pathway plays a pivotal role in senescence, in mouse cells, the ARF-p53 pathway is essential and $p16^{Ink4a}$ is dispensable for senescence (28, 29). We show here that HuR maintains a replicative life span by repressing expression of the $p19^{ARF}$ tumor suppressor in mouse embryonic fibroblasts (MEFs). RNA

Received 19 September 2012 Returned for modification 24 October 2012
Accepted 7 March 2013
Published ahead of print 18 March 2013
Address correspondence to Masataka Sugimoto, msugimot@ncgg.go.jp.
* Present address: Hiroyuki Kawagishi, Center for Molecular Medicine, National Heart, Lung and Blood Institute, Bethesda, Maryland, USA.
H.K. and M.H. contributed equally to this work.

doi:10.1128/MCB.01277-12

interference (RNAi)-mediated HuR silencing in MEFs prematurely induces cellular senescence by activating the ARF-p53 pathway. In *HuR*-depleted cells, p19^{ARF} levels, but not p16^{Ink4a} levels, are increased due to enhanced translation of *ARF* mRNA. HuR associates weakly with the 5′UTR of *ARF* mRNA in living cells. In the absence of HuR, *ARF* mRNA accumulates in the nucleolus, where it associates with nucleolin, and nucleolin is required for p19^{ARF} induction in HuR knockdown cells. Translational regulation is also observed *in vivo*, and adipose-specific *HuR* knockouts revealed progressive insulin resistance, with concomitant increased expression of p19^{ARF}. Thus, HuR translationally represses p19^{ARF} expression under normal conditions, thereby inhibiting cellular senescence and maintaining tissue functions *in vivo*.

MATERIALS AND METHODS

Cells and culture conditions. NIH 3T3 and 293T cells were maintained in Dulbecco's modified Eagle's medium (DMEM) supplemented with 10% fetal calf serum (FCS) and 100 U/ml penicillin-streptomycin. MEFs were cultured in medium supplemented with 0.1 mM nonessential amino acids, 55 μM 2-mercaptoethanol, and 10 μg/ml gentamicin instead of penicillin and streptomycin. To analyze mRNA or protein stability, cells were treated with 2 μg/ml of actinomycin D or 100 μg/ml of cycloheximide (CHX), respectively. To induce adipocytic differentiation, cells were kept confluent for 2 days and switched to differentiation medium (DMEM containing 5 μg/ml insulin, 1 μM dexamethasone, and 0.5 mM 3-isobutyl-1-methylxanthine [IBMX; Sigma Chemicals, St. Louis, MO]). For 5-ethynil-2′-deoxyuridine (EdU) staining, cells were pulse-labeled with 10 μM EdU for 45 min. Labeled cells were visualized using the Click-iT EdU Alexa Fluor imaging kit according to the manufacturer's instructions (Life Technologies, Carlsbad, CA).

Senescence-associated β-galactosidase and Oil Red O staining. Cells were washed in phosphate-buffered saline (PBS), fixed for 3 to 5 min (room temperature) in 2% formaldehyde-0.2% glutaraldehyde, washed, and incubated at 37°C with β-galactosidase (β-Gal) stain solution containing 1 mg of 5-bromo-4-chloro-3-indolyl-β-D-galactoside, 40 mM citric acid-sodium phosphate (pH 6.0), 5 mM potassium ferrocyanide, 5 mM potassium ferricyanide, 150 mM NaCl, and 2 mM $MgCl_2$. Staining was evident after 12 to 16 h (2). To stain adipocytes, cells were washed twice with PBS and then incubated with 60% filtered Oil Red O solution (3 mg/ml of 2-propanol) for 30 min at 37°C. Cells were washed with 60% 2-propanol briefly and then with water before visualization. Phase-contrast images were taken with a Plan FI 40×/0.60 lens (Olympus, Tokyo, Japan) at ambient temperature using an inverted microscope (model IX71; Olympus) equipped with a DP70 digital camera system (Olympus). Images were acquired using DP Controller software (Olympus).

Plasmids, transfection, retrovirus production, and infection. Mouse *ARF* and *Ink4a* cDNAs were obtained by PCR using the following primers: for full-length *ARF*, 5′-AAGGATCCTCTCGAGGTGCCTCAACGCC-3′ (sense) and 5′-AACTCGAGGACATTTTAAAAAGTATC-3′ (antisense); for Δ3′UTR *ARF*, the full-length sense primer and 5′-AAACTCGAGCT ATGCCCGTCGGTCTGGGC-3′ (antisense); for Δ5′UTR *ARF*, 5′-AAG GATCCATGGGTCGCAGGTTCTTGG-3′ (sense) and the full-length antisense primer; for full-length *Ink4a*, 5′-AAGGATCCACTGGTCACACG ACTGGGC-3′ (sense) and 5′-AAGAATTCGACATTTTAAAAAGTAT C-3′ (antisense); and for the *Ink4a* open reading frame (ORF), 5′-AAGG ATCCATGGAGTCCGCTGCAGACAG-3′ (sense) and 5′-AAGAATTCT TAGCTCTGCTCTTGGG-3′ (antisense). PCR products were digested with BamHI and XhoI (*ARF*) or BamHI and EcoRI (*Ink4a*) and cloned into a pcDNA3 vector (Life Technologies). For *ARF*-MS2, *ARF* cDNA (full length or Δ5′UTR) was cloned into the BamHI/XbaI sites of pcDNA3.1 Hygro (Life Technologies). The plasmid was then digested with NotI and XbaI, and annealed oligonucleotides, including a 2×MS2 tag sequence (sense, GGCCGCAAACATGAGGATCACCCATGTCCAT GGTCGACGAGCTCAAACATGAGGATCACCCATGTCT, and antisense, CTAGAGACATGGGTGATCCTCATGTTTGAGCTCGTCGA CCATGGACATGGGTGATCCTCATGTTTGC), were ligated. MS2-enhanced green fluorescent protein (EGFP)-nuclear localization signal (NLS) cDNA (30) and GFP-L10a expression plasmids were provided by Takashi Funatsu (University of Tokyo) and Leo Tsuda (National Center for Geriatrics and Gerontology), respectively. GFP-L10 cDNA was cloned into a murine stem cell virus (MSCV) vector.

For knockdown of nucleolin, 1 million MEFs were plated in a 10-cm-diameter dish and cultured in a medium without antibiotics. Synthetic small interfering RNA (siRNA) (Thermo Fisher Scientific, Lafayette, CO) was transfected using DhamaFect1 (Thermo Fisher Scientific) according to the manufacturer's instructions. Cells were collected at 48 h posttransfection for subsequent analysis.

For retrovirus production, 293T cells were transfected with retroviral expression plasmids together with helper plasmids, as described previously (31). Culture supernatants were harvested 24 to 60 h after transfection, pooled, and stored on ice. Exponentially growing cells in 10-cm-diameter culture dishes were infected with 3 ml of a fresh virus-containing supernatant in complete medium containing 8 μg/ml Polybrene. Infection was confirmed either by GFP expression or by selection for drug resistance.

RNA analyses. RNAs were prepared from cells or immune complexes using TriPure isolation reagent (Roche, Indianapolis, IN), reverse transcribed using a PrimeScript reverse transcriptase (RT) reagent kit with the genomic DNA (gDNA) Eraser (TaKaRa, Shiga, Japan), and subjected to PCR using the following primers: for *PAI-1*, 5′-TCAGAGCAACAAGTT CAACTACACTGAG-3′ (sense) and 5′-CCCACTGTCAAGGCTCCATC ACTTGCCCCA-3′ (antisense); for *HuR*, 5′-TTGGGCTACGGTTTT GTGAAC-3′ (sense) and 5′-CCCACTGATGTATAAGTTGGCAT-3′ (antisense); for *ARF*, 5′-GCCGCACCGGAATCCT-3′ (sense) and 5′-TT GAGCAGAAGAGCTGCTACGT-3′ (antisense); for *Ink4a*, 5′-CCCAAC GCCCCGAACT-3′ (sense) and 5′-GCAGAAGAGCTGCTACGTGAA-3′ (antisense); for c-*myc*, 5′-TCTATTTGGGGACAGTGTTC-3′ (sense) and 5′-GGTCATAGTTCCTGTTGGTG-3′ (antisense); for *p53*, 5′-TGGAGA GTATTTCACCCTCAAGA-3′ (sense) and 5′-CTCCTCTGTAGCATGG GCATC-3′ (antisense); for β-*actin*, 5′-CTAAGGCCAACCGTGAAAA G-3′ (sense) and 5′-ACCAGAGGCATACAGGGACA-3′ (antisense); for 18S rRNA 5′-AGTCCCTGCCCTTTGTACACA-3′ (sense) and 5′-GATC CGAGGGCCTCACTAAAC-3′ (antisense); for *AUF-1*, 5′-TTTCTCCAG ACACACCTGAAGA-3′ (sense) and 5′-CTGTTCCTTTGACATGGCTA CTT-3′ (antisense); and for *GFP*, 5′-TCTGCACCACCGGCAAGCTG-3′ (sense) and 5′-TGCGCTCCTGGACGTAGCCT-3′ (antisense). Real-time PCR analysis was carried out on a Chromo4 real-time PCR system (Bio-Rad, Hercules, CA).

Immunoblotting and preparation of cytoplasmic and nuclear fractions. Cell lysates were separated by SDS-PAGE and transferred to polyvinylidene difluoride (PVDF) membranes (Millipore, Billerica, MA). Proteins were detected with antibodies to γ-tubulin (GTU-88; Sigma Chemicals, St. Lois, MO), p19^{ARF}, p16^{Ink4a}, HuR, nucleolin, CDK4, lamin A/C, GFP, α-tubulin, peroxisome proliferator-activated receptor gamma (PPARγ) CCAAT/enhancer binding protein α (C/EBPα), C/EBPβ, C/EBPδ (5-C3-1, M-156, 3A2, MS-3, C-22, H-110, FL, B-7, E-8, 14AA, C-19, and C-22; all from Santa Cruz Biotechnology, Santa Cruz, CA), RPL10 (Atlas Antibodies, Stockholm, Sweden), RPL11 (3A4A7; Life Technologies), and RPS6 (54D2; Cell Signaling Technology, Danvers, MA). The intensities of the bands were determined using NIH's ImageJ. Cytoplasmic and nuclear fractions were generated using a Paris kit (Life Technologies).

Immunoprecipitation/RT-PCR. To analyze ribosome-mRNA association, cells were incubated in the presence of 0.1 mM CHX for 5 min and then suspended in ice-cold extraction buffer containing 10 mM HEPES-KOH (pH 7.4), 150 mM KCl, 5 mM $MgCl_2$, 0.5 mM dithiothreitol (DTT), 100 μg/ml CHX, protease inhibitors, and 40 U recombinant RNase inhibitor (Toyobo, Osaka, Japan) with a homogenizer. Homogenates were centrifuged for 10 min at 2,000 × *g* to pellet large cell debris, and Nonidet

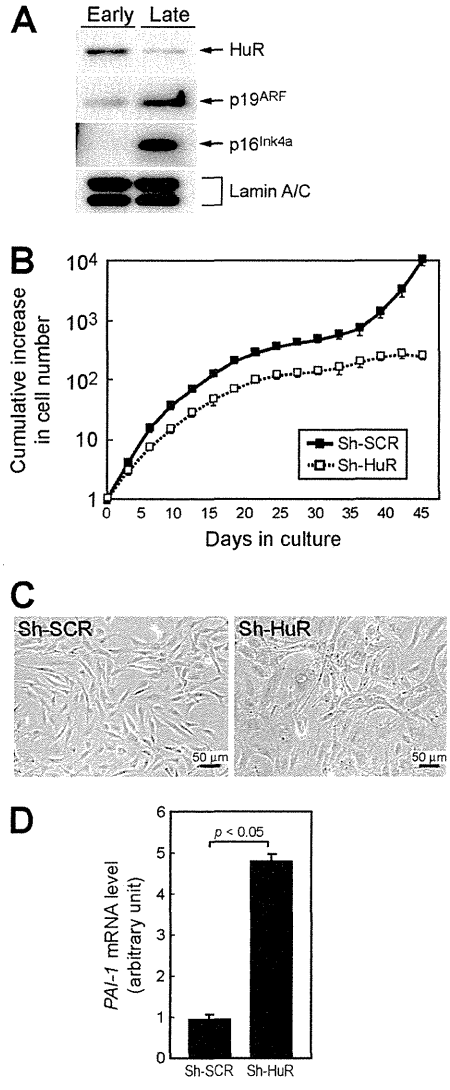

FIG 1 Loss of HuR leads to acute cellular senescence in MEFs. (A) Lysates from early-passage (passage 2 [P2]) and late-passage (P10) MEFs were analyzed for expression of the indicated proteins by immunoblotting. Lamin A/C was used as a loading control. (B) Wild-type MEFs infected with control (sh-SCR) or sh-HuR retroviruses were cultured by the NIH 3T3 protocol. Error bars represent standard errors of the means (SEM) of results from triplicate wells. (C) Cells (10 days postinfection) were stained with SA-β-Gal. (D) Expression of *PAI-1* mRNA was analyzed by real-time PCR. Values were normalized to those for *GAPDH* in each sample. Data are representative of three independent experiments. Error bars represent SEM of results from triplicate samples.

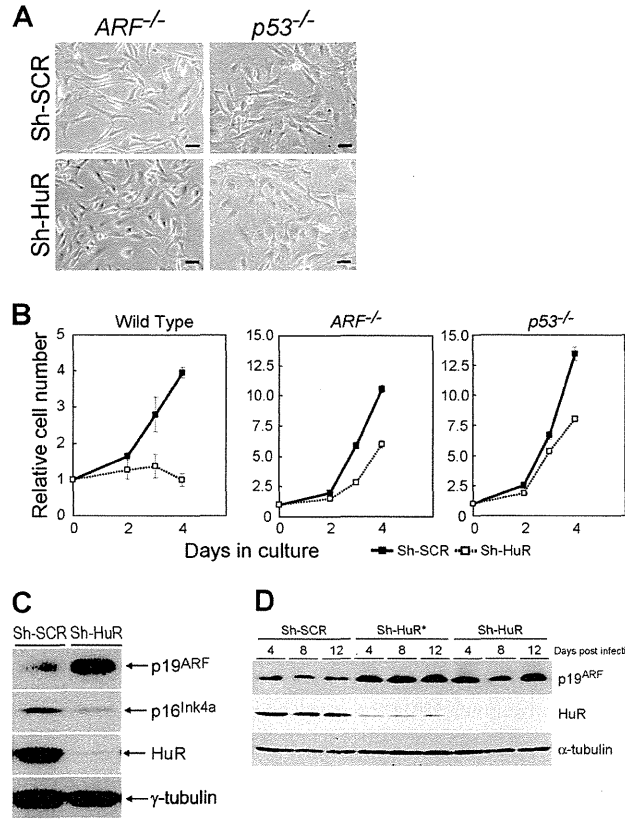

FIG 2 Senescence in HuR-depleted MEFs is dependent on the ARF-p53 pathway. (A) MEFs prepared from *ARF*- or *p53*-null animals were infected with control or sh-HuR retroviruses. Infected cells were stained for SA-β-Gal. Bars, 25 μm. (B) Control or sh-HuR MEFs with the indicated genotypes were analyzed for their growth rates. Error bars represent means ± SE of results from triplicate wells. (C) Cell lysates were prepared from wild-type MEFs infected with control or sh-HuR retroviruses. The expression of the indicated proteins was analyzed by immunoblotting. γ-Tubulin was used as a loading control. (D) Wild-type MEFs were infected with two independent sh-HuR retroviruses that target different regions of *HuR* mRNA. Cell lysates were prepared at 4, 8, and 12 days postinfection and analyzed for the expression of the indicated proteins by immunoblotting.

P-40 (NP-40; Nacalai Tesque, Kyoto, Japan) was added to the supernatant at a final concentration of 1%. After incubation on ice for 5 min, clarified lysates were cleared by centrifugation for 10 min at 13,000 × *g*. Protein A magnetic beads (Millipore) and anti-GFP (mFx73; Wako, Osaka, Japan) were preincubated at room temperature for 30 min and added to the supernatant. The mixture was incubated at 4°C with end-over-end rotation for 3 h. Beads were subsequently collected on a magnetic rack, washed three times with high-salt wash buffer (10 mM HEPES-KOH [pH 7.4], 350 mM KCl, 5 mM $MgCl_2$, 1% NP-40, 0.5 mM DTT, and 100 μg/ml CHX), and immediately placed in TriPure isolation reagent to extract bound RNAs from polysomes (32). RNA was subjected to real-time PCR analysis as described above.

For polysomal fractionation, cells were incubated in the presence of 0.1 mM cycloheximide for 5 min and lysed in a buffer containing 50 mM Tris-Cl (pH 7.5), 0.1 M NaCl, 10 mM $MgCl_2$, 2 mM DTT, 200 U/ml RNase inhibitor (Toyobo, Osaka, Japan), 100 μg/ml cycloheximide, 200 μg/ml Heparan, 0.5% NP-40, and protease inhibitors. One milliliter of lysates cleared by centrifugation was loaded onto 15-to-40% sucrose gradients in a buffer (9 ml) containing 150 mM NaCl, 5 mM $MgCl_2$, and 25 mM Tris-Cl (pH 7.5), centrifuged using an Sw41 rotor (Beckman Coulter, Fullerton, CA) (34,000 rpm, 140 min, 4 °C), and separated into 120 fractions. RNA and protein were recovered from each fraction and analyzed by real-time PCR and immunoblotting, respectively.

To analyze HuR-RNA and nucleolin-RNA complexes, cell lysates prepared using a buffer containing 50 mM HEPES (pH 7.5), 150 mM NaCl, 1 mM EDTA, 2.5 mM EGTA, 1 mM DTT, 0.2% Tween 20, 10% glycerol, and protease inhibitors were incubated at 4°C for 3 h together with protein A magnetic beads preincubated with antihemagglutinin (anti-HA) (3F10; Roche, Indianapolis, IN), anti-HuR (3A2; Santa Cruz Biotechnology), or antinucleolin (MS-3; Santa Cruz Biotechnology). Magnetic beads were washed three times with the buffer and suspended in TriPure isolation reagent to recover RNA associated with HA-tagged or endogenous HuR protein. RNAs were quantified using real-time PCR.

For UV cross-linking and immunoprecipitation, cells in a 10-cm-diameter dish were washed twice with PBS and irradiated with UV (150 mJ/cm^2) in the presence of 6 ml PBS. Irradiated cells were harvested and resuspended in a buffer containing 50 mM Tris (pH 7.4), 100 mM NaCl, 1% NP-40, 0.1% SDS, 0.5% sodium deoxycholate, 40 U/ml RNase inhibitor, and protease inhibitors. Lysates were treated with DNase I at 37°C for 3 min, cleared by centrifugation, and incubated with magnetic protein G beads pretreated with anti-HuR for 3 h at 4°C. Beads were washed twice with high-salt buffer (50 mM Tris [pH 7.4], 1 M NaCl, 1 mM EDTA, 1% NP-40, 0.1% SDS, and 0.5% sodium deoxycholate) and then twice with wash buffer (20 mM Tris [pH 7.4], 10 mM $MgCl_2$, and 0.2% Tween 20) and resuspended in PK buffer (100 mM Tris [pH 7.4], 50 mM NaCl, and 10 mM EDTA) containing proteinase K for 20 min at 37°C. An equal amount of PK buffer containing 7 M urea was added, the mixture was incubated for 20 min at 37°C, and supernatants were collected and subjected to phenol-chloroform extraction. RNAs were isolated from the aqueous phase by ethanol precipitation and subjected to real-time PCR analysis as described above.

Immunohistochemistry. Immunohistochemistry was performed on frozen sections of adipose tissue from *HuR*$^{floxed/floxed}$ (*HuR*$^{fl/fl}$) or *HuR*$^{fl/fl}$ AP2-Cre mice. Sections were fixed with 4% paraformaldehyde in PBS for 15 min, rinsed, and then placed into a covered Coplin jar containing citrate buffer (1.8 mM citric acid, 8 mM sodium citrate, pH 6.0) that had been preheated to 100°C for 30 min. Sections were rinsed in PBS for 10 min, blocked with 10% FCS in 0.1% Triton X-100–PBS for 1 h, and incubated with 5 μg/ml of anti-p19^{ARF} (5-C3-1) and anti-HuR (H-280; Santa Cruz Biotechnology) in Can Get Signal Solution A (Toyobo) at 4°C overnight. Proteins were visualized with Cy3- or Alexa Fluor 488-labeled secondary antibodies (Jackson ImmunoResearch, West Grove, PA), and slides were mounted using Vectashield and DAPI (4′,6-diamidino-2-phenylindole; Vector Laboratories, Burlingame, CA). Fluorescence images were taken with a Nikon CFI Plan Apo λ 40×/0.95-numerical-aperture lens at ambient temperature using an inverted microscope (Biorevo BZ-9000; Keyence, Osaka, Japan). Images were acquired using BZ-II Viewer software (Keyence).

Insulin and glucose tolerance tests. Animals were fasted for 4 h (for the insulin test) or overnight (for the glucose test) and intraperitoneally injected with insulin (0.75 unit/kg of body weight) or glucose (1 g/kg). Following these injections, tail vein blood (approximately 5 μl) was collected, and glucose was measured using a glucose meter (LifeScan, Milpitas, CA).

RESULTS

HuR regulates the replicative senescence of murine fibroblasts. HuR levels decline during senescence in human fibroblasts (22). We checked HuR levels in early- and late-passage mouse embryonic fibroblasts. As in human fibroblasts, HuR was downregulated in senescent MEFs where p19^{ARF} and p16^{Ink4a} levels were increased (Fig. 1A). To test if downregulation of HuR was sufficient to induce replicative senescence, MEFs were infected with retroviruses encoding short hairpin RNA (shRNA) that inhibits short hairpin HuR (sh-HuR) expression or control sh scramble (sh-SCR) (33). Infected cells were selected with puromycin and cultured according to the NIH 3T3 protocol (34). As shown in Fig. 1B, HuR knockdown cells had much shorter replicative life spans than control shRNA-expressing cells, and these cells showed the typical characteristics of cellular senescence, including a flattened shape and increased activity of senescence-associated β-galactosidase (SA-β-Gal) (Fig. 1C). In addition, another senescence marker, *plasminogen activator inhibitor-1* (*PAI-1*), was increased in HuR-depleted cells (Fig. 1D) (35). These data suggest that loss of HuR results in acute cellular senescence in mouse fibroblasts.

The ARF-p53 pathway plays an essential role in mouse cellular senescence. *ARF*- or *p53*-null cells do not undergo cellular senescence upon serial passage or oncogenic activation (36–39). To clarify the roles of the ARF-p53 pathway in the senescence of HuR knockdown MEFs, cells derived from *ARF*$^{-/-}$ or *p53*$^{-/-}$ animals were infected with retroviruses encoding sh-SCR or sh-HuR. Unlike in wild-type MEFs, no SA-β-Gal staining was observed in *ARF*$^{-/-}$ and *p53*$^{-/-}$ cells (Fig. 2A). HuR depletion consistently caused significant cell growth arrest only in wild-type MEFs, and *ARF*- or *p53*-null cells continued to proliferate irrespective of HuR status (Fig. 2B). However, HuR knockdown had a weak growth-inhibitory effect in these cells, which is consistent with earlier reports showing that HuR targets several growth-related genes (40). These results suggest that cellular senescence induced by HuR depletion is strictly dependent on the ARF-p53 pathway, while other factors may also be involved in cell growth regulation by HuR.

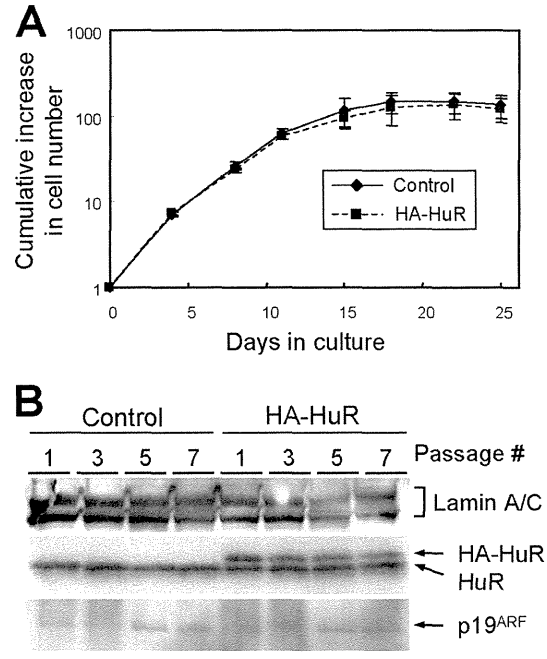

FIG 3 HuR overexpression does not affect p19^{ARF} levels or replicative life spans. (A) Wild-type MEFs were infected with retroviruses encoding GFP (control) or HA-HuR. Infected cells were cultured by the NIH 3T3 protocol. Error bars represent SEM of results from triplicate wells. (B) Cell lysates were prepared at the indicated passage numbers. The expression of the indicated proteins was analyzed by immunoblotting. Lamin A/C was used as a loading control.

p19^{ARF} is induced in HuR knockdown cells. During cellular senescence, p19^{ARF} and p16^{Ink4a} levels are increased and lead the activating signals to p53 and pRb, respectively (41). Since senescence induced by HuR depletion requires *ARF* (Fig. 1C and 2A), we checked the levels of these proteins in control and sh-HuR MEFs. Loss of HuR expression led to a significant increase in p19^{ARF} levels (Fig. 2C), while p16^{Ink4a} levels were not increased in these cells. Similar results were obtained using another shRNA, one that targets different regions of the *HuR* gene (33), confirming that increased levels of p19^{ARF} were not due to the off-target effects of sh-HuR (Fig. 2D). On the other hand, overexpression of HuR did not affect either the cells' replicative life span or p19^{ARF} levels (Fig. 3A and B).